Electronic Supplementary Materials

Differential Cell-Matrix Mechanoadaptations and Inflammation Drive Regional Propensities to Aortic Fibrosis, Aneurysm, or Dissection in Hypertension

M.R. Bersi[1], R. Khosravi[1], A.J. Wujciak[1], D.G. Harrison[2], J.D. Humphrey[1,3,*]

[1]Department of Biomedical Engineering
Yale University, New Haven, CT, USA

[2]Departments of Medicine and Pharmacology,
Vanderbilt University, Nashville, TN, USA

[3]Vascular Biology and Therapeutics Program,
Yale School of Medicine, New Haven, CT, USA

[*]Address for Correspondence:

J.D. Humphrey, Ph.D.
Department of Biomedical Engineering
212 Malone Engineering Center
Yale University, New Haven, CT 06520-8260
(P) +1-203-432-6428
(F) +1-203-432-0030
jay.humphrey@yale.edu

Supplemental Methods

Animal Model. All animal studies were approved by the Institutional Animal Care and Use Committee of Yale University. Hypertension was induced in male apolipoprotein-E null mice (*ApoE*$^{-/-}$, Jackson Laboratories) at 19.4±0.02 weeks of age via chronic infusion of angiotensin II (AngII; Sigma-Aldrich) at a continuous rate of 1000 ng/kg/min for up to 4 weeks using an osmotic mini-pump (Model #2004, Alzet). Using a sterile technique, the pump was implanted subcutaneously on the flank while the mice were under a surgical plane of anesthesia (2-3% isoflurane for induction, with 0.6 L/min of 100% O_2). Buprenorphine (0.05-0.1 mg/kg s.c.) was injected pre- and post-operatively, then as needed thereafter. Mice were allowed to recover and ambulate within a normal cage with free access to water and normal chow. Blood pressure was measured at specific infusion times (Figure S1, Table S1) using a CODA tail-cuff system (Kent Scientific) and standard methods[1]. At the prescribed endpoint (0, 4, 7, 14, 21, 28, or 224 days post-surgery; Figure S2A), mice were euthanized with Beuthanasia-D (150 mg/kg i.p.) and the ascending thoracic aorta (ATA), proximal descending thoracic aorta (DTA), suprarenal abdominal aorta (SAA), and infrarenal abdominal aorta (IAA) were excised. Note that regions of the aorta with advanced disease following AngII infusion, such as aneurysm in the ATA, dissection in the SAA, or apparent aortic rupture, were excluded from all mechanical and immunohistochemical analyses to focus the present study on identifying regional differences in mechanics and inflammation that may drive disease progression, rather than on advanced disease itself.

In summary, a total of 79 animals underwent surgery to implant osmotic mini-pumps. Of these, ~18% experienced early death due to rupture. In the end, tissue from 53 implanted animals was used in the current study, from which 114 different vessels were tested (spanning 4 different regions at 6 different times, not including 0d and 224d no AngII since these groups were not AngII treated). Assuming all regions could have potentially been tested from the 79 initial animals, we were able to test only 36% (e.g., 114/316 = 0.36). That is, our overall group had over 60% ATA dilatation, SAA dissection, or death; results on the aneurysmal dilatation and dissection will be reported elsewhere. As noted previously, all 3 long-term prior-infusion mice had stable SAA dissections at the time of tissue harvest, but we only tested the non-dissected ATA, DTA, and IAA.

Biaxial Mechanical Testing. All four aortic regions (ATA, DTA, SAA, IAA; Figure S2B) were cleaned of excess perivascular tissue, and then branches, if any, were ligated using single strands from a braided 7-0 nylon suture. The nearly cylindrical specimens were cannulated on pulled glass micropipettes, secured proximally and distally with 6-0 silk suture, and tested mechanically using a custom computer-controlled biaxial device[2]. Figure S2 also shows representative video-capture images of mounted specimens from the four regions (panel C) as well as illustrative data acquired during standard mechanical testing of the DTA (panel D). Specifically, following equilibration for 15-30 minutes in a 37°C Hanks buffered solution (HBSS, Invitrogen Life Technologies), specimens were subjected to 4 preconditioning cycles consisting of pressurization from 10 to 140 mmHg while maintained near their individual estimated *in vivo* axial length[3]. HBSS reduces basal contractile tone[4], thereby focusing the mechanical analysis on the effects of extracellular matrix independent of smooth muscle cell contractility. After recording the unloaded geometry (outer diameter and axial length),

specimens were subjected to a series of 3 cyclic pressure-diameter protocols (from 10 to 140 mmHg at 95%, 100%, and 105% of the *in vivo* axial stretch; Figure S2D, top) and 4 cyclic axial force-length protocols (from 0 to f_{max} at constant pressures of 10, 60, 100, and 140 mmHg, where f_{max} ranged from 65 mN for the ATA to 40 mN for the DTA and SAA, and 30 mN for the IAA; Figure S2D, bottom). The *in vivo* axial stretch was estimated based on the axial force-pressure relationship and defined as that stretch at which changes in the transducer-measured axial force were minimal upon pressurization. The loads (pressure and axial force) and geometry (outer diameter and axial length) were recorded continuously over 2 cycles from each of the 7 mechanical testing protocols (3 pressure-diameter + 4 axial force-length). Using the assumption of isochoric deformations (incompressibility), measurements of unloaded wall thickness were combined with on-line geometric measurements to compute values of wall thickness at every quasi-statically loaded configuration[3]. The wall thickness computed for each deformed configuration was then used to compute biaxial wall stress and strain. Figure S3 shows illustrative biaxial data for all four regions from 0 to 28 days of AngII infusion for one pressure-diameter (Figure S3A, top) and one axial force-length (Figure S3A, bottom) protocol, plus the associated calculated biaxial stresses (Figure S3B, top and bottom, respectively).

Histology and Immunohistochemistry. Following mechanical testing, all vessels were unloaded and placed within a 10% neutral buffered formalin solution overnight and then stored in 70% ethanol at 4°C. Samples were embedded in paraffin, sectioned serially (5 μm thickness), and stained with Verhoeff Van Giesen (VVG), Movat's Pentachrome (MOV), or Picro-Sirus Red (PSR). Five sections were analyzed per aortic region from two representative vessels fixed after 0, 4, 14, or 28 days of AngII infusion (n = 5 x 2 = 10 images per stain per region per time = 480 sections quantified). Custom MATLAB scripts were used to extract layer-specific cross-sectional areas and wall percentages (Figures S4 and S5E-L; Table S4 – see also Figure 5 in the main text) in addition to area fractions for the primary structural constituents of the aortic wall (Figure S5A-D; Table S5 – see also Figure 2 in the main text) – elastin (φ^e), collagen (φ^c), smooth muscle (φ^m), and ground substance or glycosaminoglycans (φ^g). Medial-adventitial percentages and φ^e were averaged from VVG and MOV stained images, φ^m and φ^g were extracted from MOV images, and collagen was calculated from PSR images[5,6], assuming that the sum of these constituents comprise the entire cross-sectional area (i.e., $\varphi^e + \varphi^c + \varphi^m + \varphi^g = 1$). VVG-stained sections also revealed breaks in the elastic laminae, when present (Figure S6).

For immunofluorescence staining, cut sections were deparaffinized and rehydrated prior to heat-mediated antigen retrieval in citrate buffer for 25 minutes. Following blocking with Background Sniper (Biocare Medical) to reduce nonspecific background staining, sections were incubated overnight with antibodies for CD45 (BD Pharmingen 550539, 1:100), CD68 (Abcam ab125212, 1:1000), CD3ε (BD Pharmingen 557306, 1:50), MMP2 (Millipore AB19167, 1:400), MMP12 (Abcam ab66157, 1:500), or MMP13 (Abcam ab39012, 1:600) (cf. Figure S7). Primary antibody binding was visualized using species-specific Alexa Fluor 594–conjugated secondary antibodies (Invitrogen). Sections were mounted using ProLong Gold antifade reagent with DAPI (Invitrogen). Each tissue section was imaged under three separate fluorescent channels: red for the molecular marker of interest, green to capture elastin autofluorescence, and blue for DAPI (cell nuclei), as illustrated in Figures S4 and S7. Filter cubes used for the red (R), green (G), and blue (B) channels were U-N51005 (excitation filter 505-555 nm, emission filter 580-680 nm, dichromatic mirror 560 nm), U-MNIBA2 (excitation filter 470-490 nm, emission

filter 510-550 nm, dichromatic mirror 505 nm), and U-N31000 (excitation filter 352-402 nm, emission filter 417-477 nm, dichromatic mirror 409 nm), all from Olympus. For each primary antibody, three sections were analyzed per region from two vessels fixed after 0, 4, 14, or 28 days of AngII infusion (n = 3*2 = 6 images per stain per region per time = 576 sections quantified). Individual images from each channel (R, G, and B) were merged based on a maximum intensity projection (Figure S4C,D). Media and adventitia were segmented based on the location of the external elastic lamina in the green elastin autofluorescence images and total cell numbers and cellular densities were extracted from blue DAPI staining (Figure S4 and S8, Table S5). In addition, the density of positive red pixels (MMP-2, -12, -13) or the absolute number and density of positively stained cells (CD3, CD45, CD68) were computed separately for the media and adventitia (Table S5 – see also Figure 3 in the main text). All densities were computed based on layer-specific cross-sectional areas averaged from VVG and MOV images.

All images were acquired on an Olympus BX/51 microscope using an Olympus DP70 digital camera (CellSens Dimension) under a 20x magnification objective. Complete cross-sections of stained samples were obtained by stitching together individual sub-images (often 6, but up to 12) with either a modified feature-based panoramic image stitching algorithm (MATLAB) or the Image Composite Editor software (Microsoft Research), as needed.

Quantification of Mechanical Properties. The nonlinear passive behavior of arteries is best described using a hyperelastic constitutive framework wherein an appropriate scalar function W is defined to represent the energy stored elastically within the tissue, per unit volume, upon mechanical loading[7]. Stress and material stiffness can be computed from first and second derivatives of W, respectively, with respect to an appropriate measure of strain. Full details summarizing the nonlinear mechanics of the arterial wall can be found elsewhere[3]; for completeness, however, we list several of the primary equations here.

Motivated by histological observations of the orientations and distributions of structurally significant constituents within the murine arterial wall[4], we employed a radially homogenized, "four-fiber family" form of W to characterize the biaxial properties. This stored energy function can be written

$$W(\mathbf{C}, \mathbf{M}^i) = \frac{c}{2}(I_\mathbf{C} - 3) + \sum_{i=1}^{4} \frac{c_1^i}{4c_2^i}\left\{\exp\left[c_2^i\left(IV_\mathbf{C}^i - 1\right)^2\right] - 1\right\}, \tag{S1}$$

where c, c_1^i, and c_2^i ($i = 1,2,3,4$, to represent four distinct families of collagen fibers) are model parameters, with c and c_1^i having units of stress (kPa) while c_2^i is dimensionless. The right Cauchy-Green deformation tensor $\mathbf{C} = \mathbf{F}^\mathrm{T}\mathbf{F}$, where $\mathbf{F} = \mathrm{diag}(\lambda_r, \lambda_\vartheta, \lambda_z)$ is the deformation gradient tensor, with incompressibility requiring $\lambda_r = 1/(\lambda_\vartheta \lambda_z)$. $\mathbf{M}^i = [0, \sin\alpha_0^i, \cos\alpha_0^i]$ represents a unit vector in the direction of the i^{th} fiber family, with the fiber angle α_0^i computed relative to the axial direction in the reference configuration. Thus, axial and circumferential fiber families are oriented at $\alpha_0 = 0°$ and $\alpha_0 = 90°$, respectively. $I_\mathbf{C} = \mathrm{tr}(\mathbf{C})$ and $IV_\mathbf{C}^i = \mathbf{M}^i \cdot \mathbf{C}\mathbf{M}^i$ can be written in terms of stretch ratios, namely

$$I_\mathbf{C} = \lambda_\vartheta^2 + \lambda_z^2 + \frac{1}{\lambda_\vartheta^2 \lambda_z^2}, \quad IV_\mathbf{C}^i = \lambda_\vartheta^2 \sin^2\alpha_0^i + \lambda_z^2 \cos^2\alpha_0^i, \tag{S2}$$

Using Equation S1, the Cauchy stress tensor $\mathbf{t}$ can be computed as

$$\mathbf{t} = -p\mathbf{I} + 2\mathbf{F}\frac{\partial W}{\partial \mathbf{C}}\mathbf{F}^\mathrm{T}, \tag{S3}$$

where p is a Lagrange multiplier that enforces incompressibility, **I** is the second order identity tensor, and the superscript T denotes the tensor transpose operation.

Biaxial Cauchy stresses were computed from on-line measurements of deformation (outer diameter and axial stretch) and applied loads (pressure and axial force) and confirmed using the identified values of the 8 model parameters in *W* based on data from all 7 biaxial testing protocols (cf. Figure S2). Specifically, best-fit values of these parameters were identified using a nonlinear regression that sought to minimize an objective function defined by the normalized sum-of-the-squared differences between experimentally measured and theoretically predicted pressures and axial forces[3]. Neglecting the radial stress relative to the circumferential and axial stresses, we adopted a 2-D formulation whereby theoretical expressions for pressure and axial force were obtained by inverting global equilibrium equations for the mean wall stress (denoted $< \cdots >$). Namely,

$$\sigma_\vartheta = \langle t_{\vartheta\vartheta} \rangle = \frac{Pa}{h} \ , \qquad \sigma_z = \langle t_{zz} \rangle = \frac{f}{\pi h(2a+h)} \tag{S4}$$

were solved for the transmural pressure *P* and the total axial force on the vessel $f = f_T + \pi a^2 P$, where f_T represents the transducer-measured axial force; a and h are the loaded inner radius and wall thickness, respectively. Additionally, the linearized stiffness tensor ($\mathscr{C}_{ijkl}$) was computed as,

$$\mathscr{C}_{ijkl} = 2\delta_{ik}F^o_{lA}F^o_{jB}\frac{\partial W}{\partial C_{AB}} + 2\delta_{jk}F^o_{iA}F^o_{lB}\frac{\partial W}{\partial C_{AB}} + 4F^o_{iA}F^o_{jB}F^o_{kP}F^o_{lQ}\frac{\partial^2 W}{\partial C_{AB}\partial C_{PQ}}\bigg|_{\mathbf{C}^o} , \tag{S5}$$

where δ_{ij} are components of **I**, $\mathbf{F}^o$ is the deformation gradient tensor that maps the reference configuration into a finitely deformed *in vivo* configuration, and $\mathbf{C}^o$ is the corresponding right Cauchy-Green tensor[8].

Given the final set of best-fit material parameter values (Table S3), we computed deformation-dependent values of biaxial wall stress (Equation S4), biaxial material stiffness (Equation S5), and elastic energy storage (Equation S1). See Figures 1 (in the main text), S3, and S9. To facilitate consistent comparisons across all regions and times, all mechanical metrics (Table S2) were evaluated at the systolic pressure measured after the specific period of AngII infusion (e.g., 0, 4, 7, 14, 21, 28 or 224 days; Figure S1, Table S1). Combining geometric and material metrics, we also computed two measures of structural stiffness: the structural parameter known as distensibility, defined as

$$\mathcal{D} = [d_{sys} - d_{dias}]/[(d_{dias})(P_{sys} - P_{dias})], \tag{S6}$$

where d is the outer diameter and *P* is the blood pressure at systole (*sys*) or diastole (*dias*), and a structural stiffness (in N/m) computed as $h\mathscr{C}_{ijkl}$, where h is wall thickness and $\mathscr{C}_{ijkl}$ is the material stiffness, each evaluated at a systole (Tables S2A-D). The schematic diagram in Figure S2D summarizes the data needed to quantify the bulk mechanical properties.

Statistics. Data are presented as mean ± standard error of the mean (SEM). Comparisons of geometric and material metrics within a given region (ATA, DTA, SAA, or IAA) were assessed over time (0, 4, 7, 14, 21, 28, or 224 days) using one-way ANOVA with a post-hoc Tukey HSD test for multiple comparisons. Layer-specific differences (medial-adventitial cross-sectional area and immuno-histological expression) within a given region (ATA, DTA, SAA, or IAA) were assessed over time (0, 4,

14, or 28 days) and compared using two-way ANOVA followed by post-hoc Tukey HSD tests for multiple comparisons.

Potential correlations between measured variables were assessed using the Pearson product-moment correlation coefficient (R) and the non-parametric Spearman rank correlation coefficient (ρ) (Figure S10 and Tables S6A-N – see also Figure 4A,B in the main text). For individual correlations, the 95% bivariate confidence ellipse is shown (Figures S10), with principal axes corresponding to eigenvalues of the covariance matrix between the two independent variables. Lower diagonal matrices of Pearson correlation coefficients were assembled based on the covariance of individual pairwise correlations.

To increase confidence in the identified correlation p-values, and to account for multiple comparisons among correlations, permutation testing without replacement was performed for a total of 30,000 iterations. This permutation scheme provides sufficient confidence that the identified p-value for a given correlation will have no more than 5% error at a significance level of $\alpha = 0.05$. Namely, the p-value error can be expressed as $p_{err} = 2\sqrt{\alpha(1-\alpha)}/K$, where K is the number of permutations and α is the significance level[9]. Multiple values of significance were considered in all statistical analyses ($p <$ 0.1, 0.05, 0.01 and 0.001). For correlations between two independent metrics, significance was determined based on the location of the original R-value in a distribution of permuted R-values. Specifically, significance levels were determined based on a given percentage (i.e., $p = 0.05$, 0.01, or 0.001) away the tails of the distribution of permuted R-values (Figure S10C,E). Significant differences are indicated in all figures and tables as appropriate.

Supplemental Discussion

There is considerable evidence that vascular smooth muscle cells and fibroblasts are highly mechanosensitive[10,11]. Since the seminal paper by Glagov and colleagues[12], organ culture[13] and cell culture[14] studies confirm that increased pressure-induced or stretch-induced stresses increase extracellular matrix production by these cells. In particular, stressed vascular smooth muscle cells and fibroblasts produce fibronectin, collagen, and glycosaminoglycans, in part, via Ang II / transforming growth factor-beta (TGF-β) signaling pathways. Importantly, increased stresses also increase matrix metalloproteinase (MMP) activity[15,16]. That is, mechanical stress stimulates both deposition and degradation of extracellular matrix, each of which are needed to effect adaptive growth and remodeling[17]. These findings have been supported by *in vivo* studies as well. In particular, following transverse aortic constriction (TAC), blood pressure increases acutely in proximal sites and decreases in distal sites[6,18,19]. Regions of initially increased pressure-induced wall stress experience a matrix turnover that is driven in large part by Ang II / TGF-β signaling. Indeed, the importance of mechano-sensing and mechano-regulation of extracellular matrix remodeling was shown definitively using an α1 integrin knockout mouse[20] wherein Ang II induced hypertension did not lead to increased wall thickness in the carotid artery of the mutant mice.

Notwithstanding the fundamental roles of AngII and TGF-β in driving matrix production, both *in vitro*[14,21] and *in vivo*[18] studies show that AT_1R antagonists and TGF-β neutralizing antibodies can only attenuate, not block, changes in extracellular matrix turnover / accumulation. Hence, additional biomolecules and pathways are likely involved in the *in vivo* remodeling process. Chronic AngII

infusion has proven to be a useful model to investigate *in vivo* mechanisms of hypertension-induced vascular remodeling, but the interpretation of results can be complicated by the myriad actions of AngII signaling. AngII is a potent vasoconstrictor of peripheral vessels, but it is also a direct stimulant of matrix production[13,21] and it is pro-inflammatory[22,23]. For example, AngII can lead to the production of chemokines and cytokines, such as MCP-1 and IL-6, among others, which facilitate the recruitment of inflammatory cells that can further drive matrix production and removal[24,25]. That AngII differentially affects large artery vasoconstriction due to differences in AT_{1b} receptor densities[26], which affects local wall stress independent of increasing systemic blood pressure[27], further complicates data interpretation. Thus, delineating mechanical versus inflammatory contributions to the observed vascular remodeling can be a challenge.

The present data (cf. Figure 4 in the main text) show for the first time, however, that the observed aortic wall remodeling arises from an early mechano-mediated adaptive response (< 14 days), followed by an immuno-mediated maladaptive response (> 14 or 21 days). The latter has been suggested to depend on T-cells and IL-17a production in DOCA-salt and Ang II induced hypertension[25], consistent with our results delineating the time course of $CD45^+$ cell infiltration. This finding is particularly interesting because the early mechano-mediated remodeling manifested independent of inflammatory infiltrates despite the continuous infusion of a pro-inflammatory agent to increase the mechanical stimulus (i.e., blood pressure).

There is clearly a need to understand better the roles of paracrine interactions (between endothelial cells, smooth muscle cells, fibroblasts, and inflammatory cells) in the complex mechano-, then immuno-dominated processes of fibrosis and dissection. Similarly, there is a need to understand better any initial phenotypic differences as well as regionally dependent phenotypic modulation of mural cells. That the ATA alone experiences smooth muscle hyperplasia rather than hypertrophy in response to AngII-induced hypertension may relate to the distinct inability of this region alone to maintain circumferential material stiffness and thus have a propensity towards aneurysmal dilatation. That the IAA alone has a high AT_{1b} receptor density[28,26], and thus is able to contract against the exogenous AngII-induced elevation in blood pressure, may relate to the distinct ability of this region to maintain wall stress and mechano-adapt, thereby not thickening adversely. These and other regional differences in mechanobiological responses need to be explored in greater detail. Given inherent differences in different mouse models, regional comparisons are best accomplished using single models subjected to different perturbations.

Funding

This work was supported, in part, by NIH grants R01 HL086418, R01 HL105297, and U01 HL116323 (to JDH) and MSTP T32 GM07205.

Supplemental References

1. Daugherty, A., Rateri, D., Hong, L. & Balakrishnan, A. Measuring blood pressure in mice using volume pressure recording, a tail-cuff method. *J. Vis. Exp.* 154–160 (2009).
2. Gleason, R. L., Gray, S. P., Wilson, E. & Humphrey, J. D. A multiaxial computer-controlled organ culture and biomechanical device for mouse carotid arteries. *J. Biomech. Eng.* **126,** 787 (2004).
3. Ferruzzi, J., Bersi, M. R. & Humphrey, J. D. Biomechanical phenotyping of central arteries in health and disease: advantages of and methods for murine models. *Ann. Biomed. Eng.* **41,** 1311–30 (2013).
4. Ferruzzi, J., Collins, M. J., Yeh, A. T. & Humphrey, J. D. Mechanical assessment of elastin integrity in fibrillin-1-deficient carotid arteries: implications for Marfan syndrome. *Cardiovasc. Res.* **92,** 287–95 (2011).
5. Bersi, M. R., Collins, M. J., Wilson, E. & Humphrey, J. D. Disparate changes in the mechanical properties of murine carotid arteries and aorta in response to chronic infusion of angiotensin-II. *Int. J. Adv. Eng. Sci. Appl. Math.* **4,** 228–240 (2012).
6. Eberth, J. F., Gresham, V. C., Reddy, A. K., Popovic, N., Wilson, E. & Humphrey, J. D. Importance of pulsatility in hypertensive carotid artery growth and remodeling. *J. Hypertens.* **27,** 2010–21 (2009).
7. Humphrey, J. D. *Cardiovascular Solid Mechanics: Cells, Tissues and Organs*. (Springer, 2002).
8. Baek, S., Gleason, R. L., Rajagopal, K. R. & Humphrey, J. D. Theory of small on large: Potential utility in computations of fluid-solid interactions in arteries. *Comput. Methods Appl. Mech. Eng.* **196,** 3070–3078 (2007).
9. Bishara, A. J. & Hittner, J. B. Testing the significance of a correlation with nonnormal data: Comparison of Pearson, Spearman, transformation, and resampling approaches. *Psychol. Methods* **17,** 399–417 (2012).
10. Haga, J. H., Li, Y.-S. J. & Chien, S. Molecular basis of the effects of mechanical stretch on vascular smooth muscle cells. *J. Biomech.* **40,** 947–960 (2007).
11. Chiquet, M., Gelman, L., Lutz, R. & Maier, S. From mechanotransduction to extracellular matrix gene expression in fibroblasts. *Biochim. Biophys. Acta - Mol. Cell Res.* **1793,** 911–920 (2009).
12. Leung, D. Y. M., Glagov, S. & Mathews, M. B. Cyclic stretching stimulates synthesis of matrix components by arterial smooth muscle cells in vitro. *Science* **191,** 475–477 (1976).
13. Bardy, N., Merval, R., Benessiano, J., Samuel, J. L. & Tedgui, A. Pressure and angiotensin II synergistically induce aortic fibronectin expression in organ culture model of rabbit aorta. Evidence for a pressure-induced tissue renin-angiotensin system. *Circ. Res.* **79,** 70–78 (1996).
14. Li, Q., Muragaki, Y., Hatamura, I., Ueno, H. & Ooshima, A. Stretch-induced collagen synthesis in cultured smooth muscle cells from rabbit aortic media and a possible involvement of angiotensin II and transforming growth factor-beta. *J. Vasc. Res.* **35,** 93–103 (1998).
15. Lehoux, S., Lemarié, C. A., Esposito, B., Lijnen, H. R. & Tedgui, A. Pressure-induced matrix metalloproteinase-9 contributes to early hypertensive remodeling. *Circulation* **109,** 1041–1047 (2004).
16. O'Callaghan, C. J. & Williams, B. Mechanical strain-induced extracellular matrix production by

human vascular smooth muscle cells: role of TGF-beta(1). *Hypertension* **36,** 319–324 (2000).

17. Humphrey, J. D. Mechanisms of arterial remodeling in hypertension: coupled roles of wall shear and intramural stress. *Hypertension* **52,** 195–200 (2008).

18. Kuang, S. Q., Geng, L., Prakash, S. K., Cao, J. M., Guo, S., Villamizar, C., Kwartler, C. S., Peters, A. M., Braiser, A. R. & Milewicz, D. M. Aortic remodeling after transverse aortic constriction in mice is attenuated with AT1 receptor blockade. *Arterioscler. Thromb. Vasc. Biol.* **33,** 2172–2179 (2013).

19. Menon, A., Wendell, D. C., Wang, H., Eddinger, T. J., Toth, J. M., Dholakia, R. J., Larsen, P. M., Jensen, E. S. & Ladisa, J. F. A coupled experimental and computational approach to quantify deleterious hemodynamics, vascular alterations, and mechanisms of long-term morbidity in response to aortic coarctation. *J. Pharmacol. Toxicol. Methods* **65,** 18–28 (2012).

20. Louis, H., Kakou, A., Regnault, V., Labat, C., Bressenot, A., Gao-Li, J., Gardner, H., Thornton, S. N., Challande, P., Li, Z. & Lacolley, P. Role of alpha1beta1-integrin in arterial stiffness and angiotensin-induced arterial wall hypertrophy in mice. *Am. J. Physiol. Heart Circ. Physiol.* **293,** H2597–H2604 (2007).

21. Stanley, A. G., Patel, H., Knight, A. L. & Williams, B. Mechanical strain-induced human vascular matrix synthesis: the role of angiotensin II. *J. Renin. Angiotensin. Aldosterone. Syst.* **1,** 32–35 (2000).

22. Mehta, P. K. & Griendling, K. K. Angiotensin II cell signaling: physiological and pathological effects in the cardiovascular system. *Am. J. Physiol. Cell Physiol.* **292,** C82–97 (2007).

23. Unger, T. The role of the renin-angiotensin system in the development of cardiovascular disease. *Am. J. Cardiol.* **89,** 3A–9A; discussion 10A (2002).

24. Tieu, B. C., Lee, C., Sun, H., Lejeune, W., Recinos, A., Ju, X., Spratt, H., Guo, D. C., Milewicz, D. M., Tilton, R. G. & Braiser, A. R. An adventitial IL-6/MCP1 amplification loop accelerates macrophage-mediated vascular inflammation leading to aortic dissection in mice. *J. Clin. Invest.* **119,** 3637–51 (2009).

25. Wu, J., Thabet, S. R., Kirabo, A., Trott, D. W., Saleh, M. A., Xiao, L., Madhur, M. S., Chen, W. & Harrison, D. G. Inflammation and mechanical stretch promote aortic stiffening in hypertension through activation of p38 mitogen-activated protein kinase. *Circ. Res.* **114,** 616–625 (2014).

26. Poduri, A., Owens, A. P., Howatt, D. A., Moorleghen, J. J., Balakrishnan, A., Cassis, L. A. & Daugherty, A. Regional variation in aortic AT1b receptor mRNA abundance is associated with contractility but unrelated to atherosclerosis and aortic aneurysms. *PLoS One* **7,** 1–8 (2012).

27. Humphrey, J. D. & Wilson, E. A potential role of smooth muscle tone in early hypertension: a theoretical study. *J. Biomech.* **36,** 1595–601 (2003).

28. Owens, A. P., Subramanian, V., Moorleghen, J. J., Guo, Z., McNamara, C. A., Cassis, L. A. & Daugherty, A. Angiotensin II induces a region-specific hyperplasia of the ascending aorta through regulation of inhibitor of differentiation 3. *Circ. Res.* **106,** 611–619 (2010).

Supplemental Figures

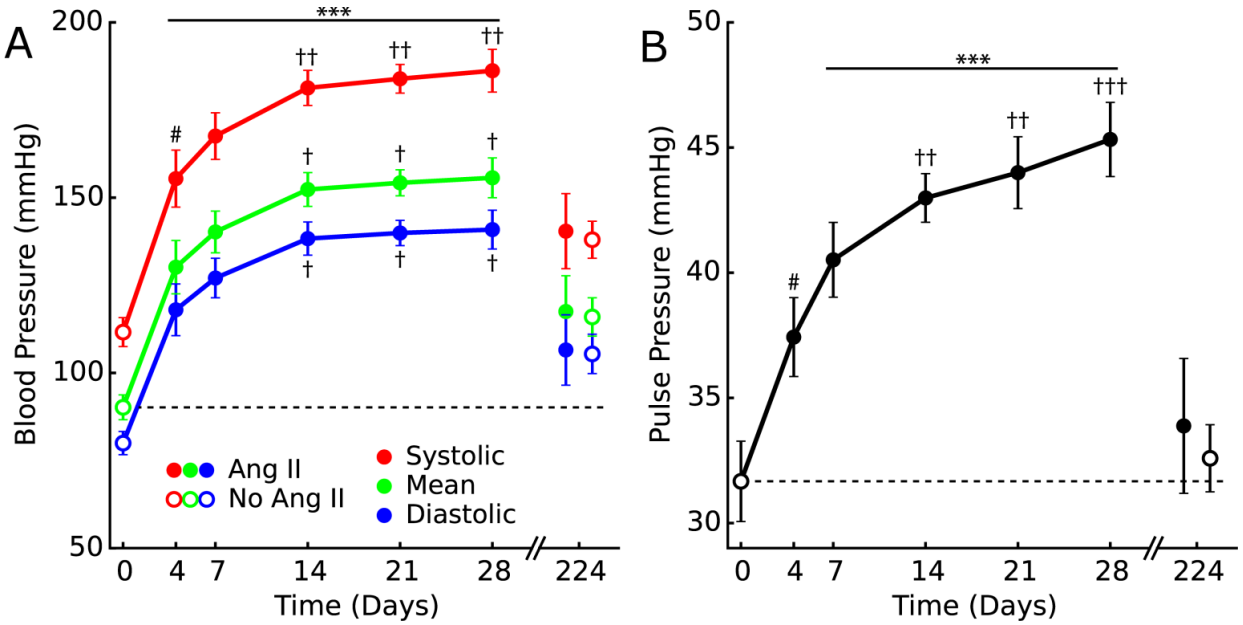

Figure S1. (A) Conscious tail-cuff measured systolic (red), mean (green), and diastolic (blue) blood pressures and (B) pulse pressures (black) at baseline (0 days) as well as 4, 7, 14, 21, 28, and 224 days post-surgery. Closed circles denote AngII infused whereas open circles denote non-AngII infused age-matched controls (n = 10-18 per group). Blood pressures nearly plateau at 14 days. Pressure values and systolic ratios (e.g., P_{sys}/P_{sys}^{0d}) are summarized in Table S1. Note that an optimally mechano-adapted large artery will have an increase in wall thickness that equals this ratio of pressures if volumetric blood flow remains unchanged[17]. *** $p < 0.001$ vs. 0 day, $^{\#}$ $p < 0.05$ vs. 28 days, and †, ††, ††† $p < 0.05$, 0.01, 0.001 vs. 224 days of no AngII.

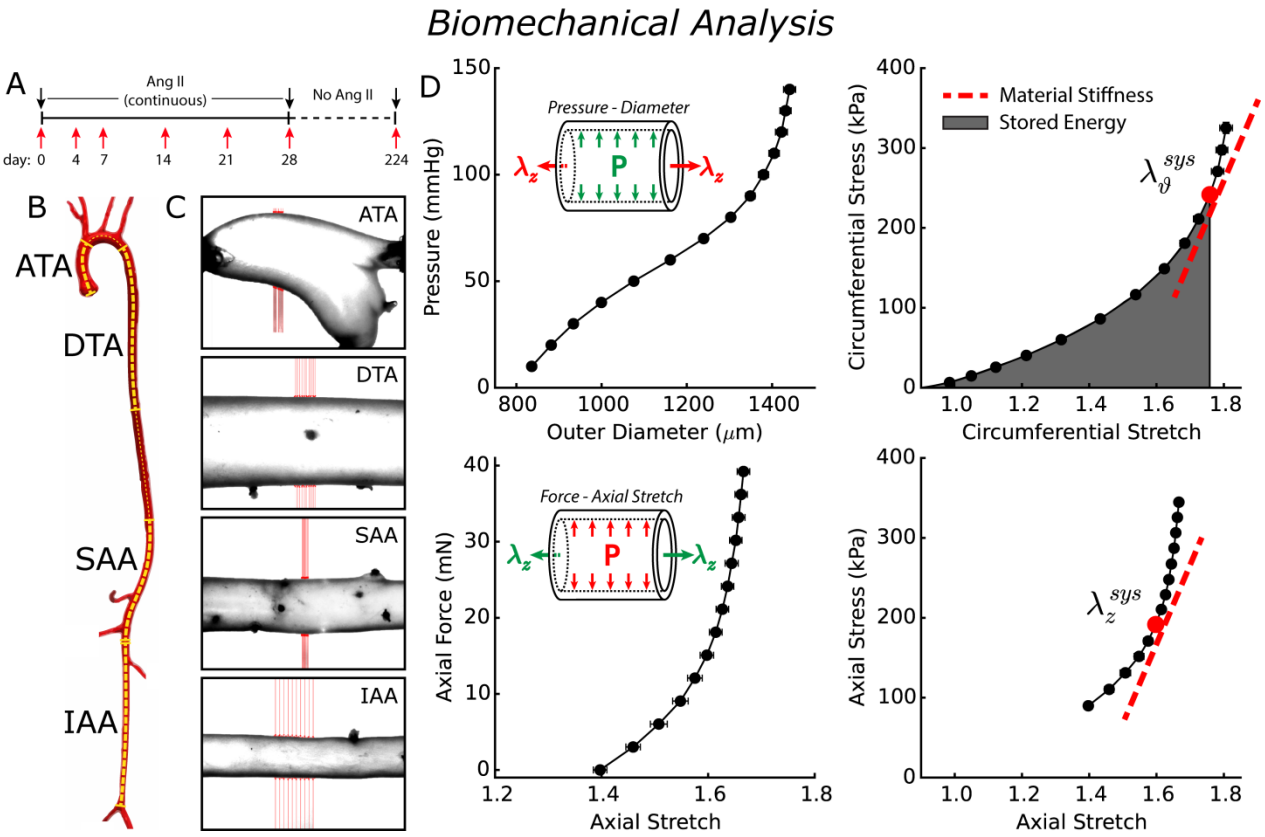

Figure S2. Overview of the experimental design, including (A) a timeline for AngII infusion and tissue harvest, (B) an illustration of the anatomical locations of the four tested regions of the aorta, and (C) representative video-capture images of a specimen from each region during mechanical testing with on-line automatic outer diameter tracing shown in red. ATA denotes the ascending thoracic aorta, DTA the proximal descending thoracic aorta, SAA the suprarenal abdominal aorta, and IAA the intrarenal abdominal aorta. Shown, too, are (D) illustrative biaxial data acquired during pressure-diameter testing at a fixed axial stretch (top left) and axial force-length testing at a fixed luminal pressure (bottom left), from which associated Cauchy stress-stretch data can be computed (top right and bottom right, respectively). Note that the elastically stored energy equals the area under a specific stress-strain surface (i.e., under the second Piola-Kirchhoff stress – Green strain surface though it is illustrated here conceptually as area under the Cauchy stress – stretch curve), but herein it is calculated directly from *W* (Equation S1). Similarly, linearized material stiffnesses are essentially the slope of the Cauchy stress-stretch surfaces at a constant fixed biaxial stretch ($\lambda_\vartheta^{sys}, \lambda_z^{sys}$)**,** though herein they are calculated via second derivatives of *W* and linearized over the in vivo range of pulse pressure (Equation S5).

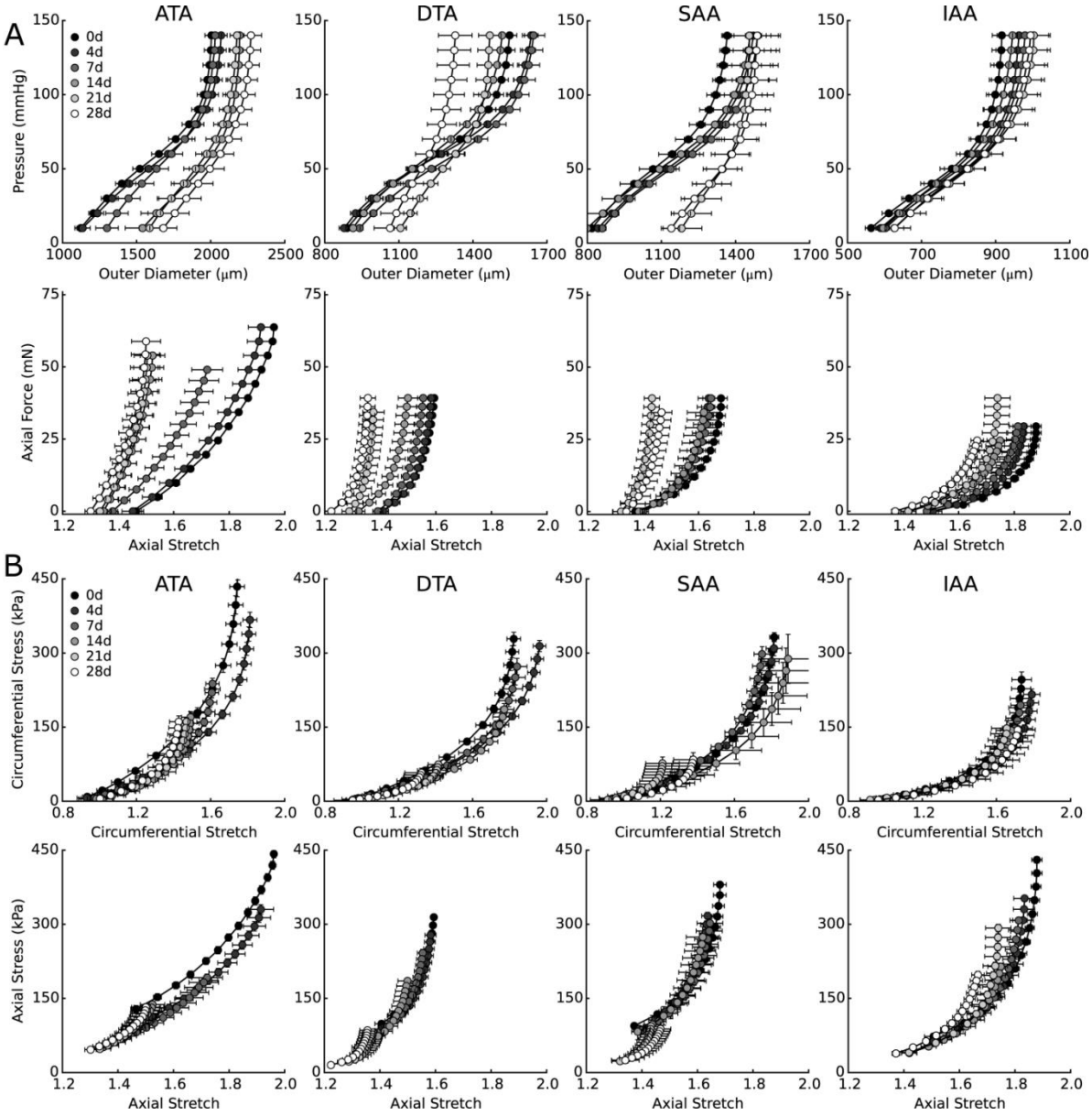

Figure S3. Average passive biaxial mechanical responses (mean ± SEM) following infusion with AngII. (A) Pressure-diameter responses at individual values of *in vivo* axial stretch (first row) and axial force-length responses at a fixed luminal pressure of 100 mmHg (second row) for all four regions (ATA, DTA, SAA, and IAA) at baseline (0 days) and 4, 7, 14, 21, and 28 days of AngII infusion (n = 4-7 per group). (B) Associated circumferential (at *in vivo* stretch; first row) and axial (at 100 mmHg; second row) Cauchy stress-stretch behaviors. Note the marked reductions in stress due to significant increases in wall thickness in all regions except the IAA (cf. Figure 1B,D,E in the main text), with IAA stresses at systolic pressures being homeostatic at later times (Table S2). All geometric and material metrics are summarized in Tables S2A-D.

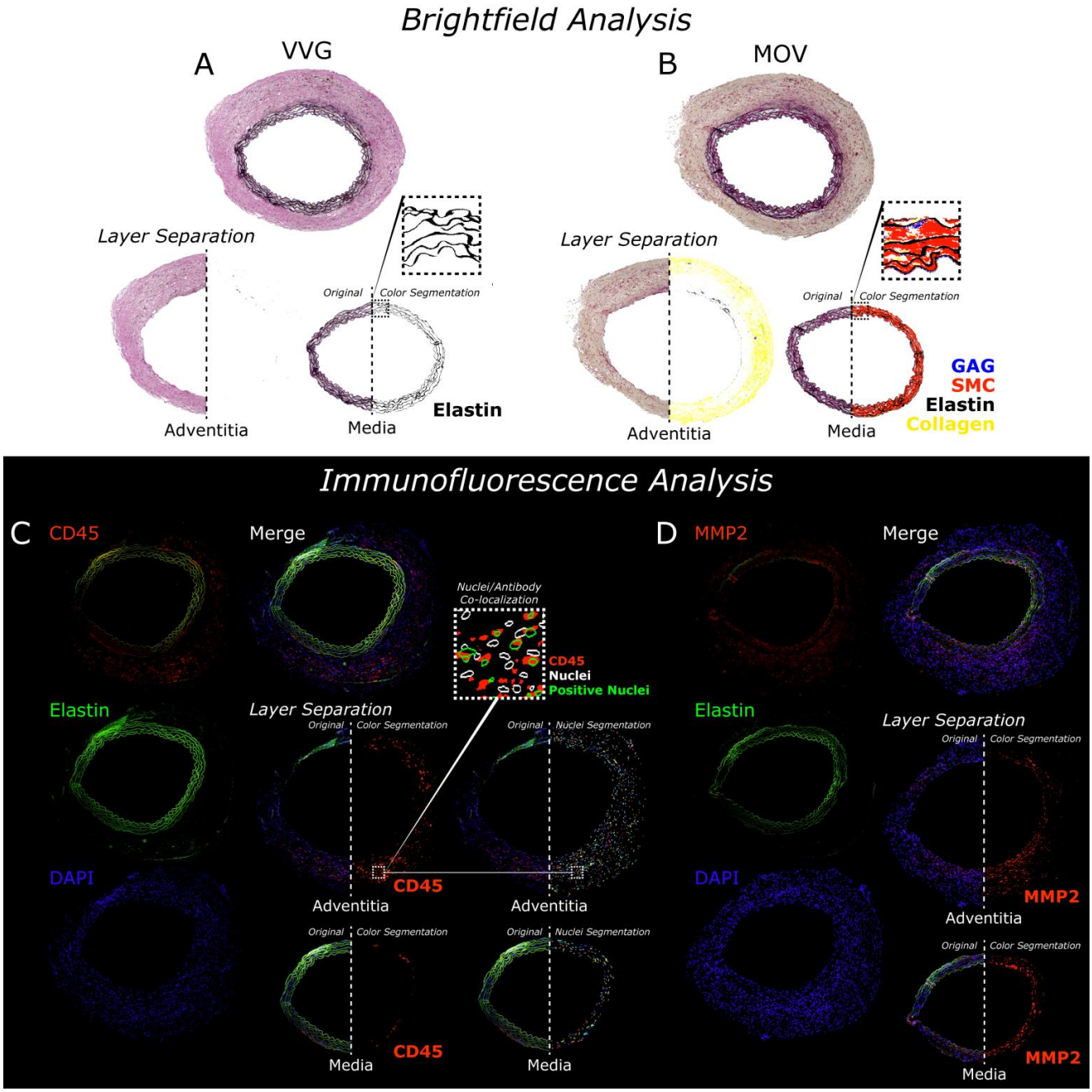

Figure S4. Overview of histological and immunohistological analyses. (A,B) Bright-field images are separated into medial and adventitial layers prior to color-based segmentations to identify constituents (see insert). VVG is Verhoeff Van Gieson and MOV is Movat's pentachrome stain. (C,D) Immuno-fluorescence images are merged prior to medial-adventitial separation. Color-based segmentation is then used to identify regions of secondary antibody staining (e.g., red for $CD45^{+}$ inflammatory cells or matrix metalloproteinases, MMPs). For cell specific markers (C), boundaries of cell nuclei are extracted from DAPI images (blue) using a modified watershed algorithm. Positive nuclei are then characterized based on co-localization of nuclei boundaries and positive antibody staining (C, insert). Split images show an original (left) and a pseudo-colored (right) cross-section highlighting either positively identified constituents or cell nuclei. Green shows elastin autofluorescence.

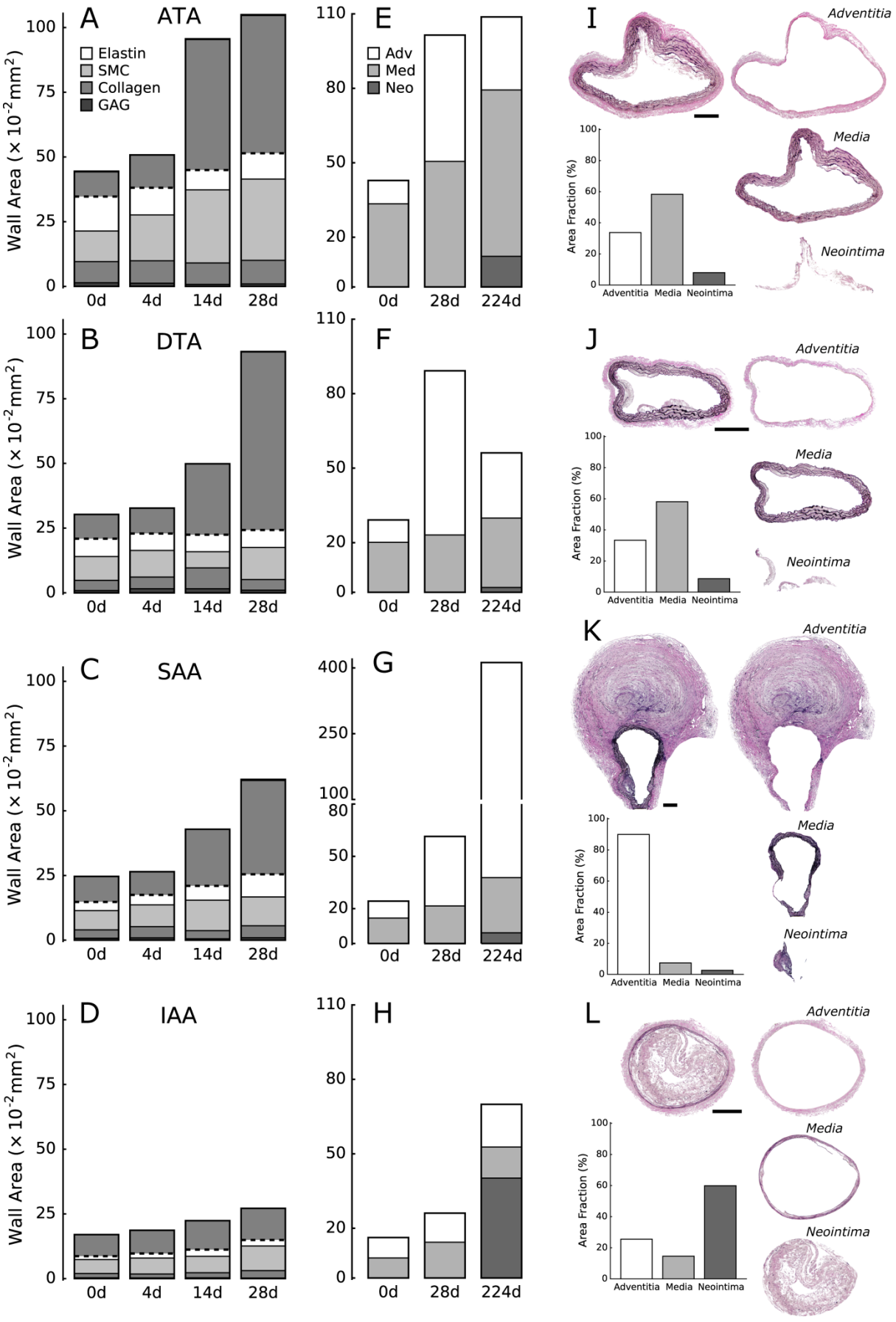
A
ATA
Elastin
SMC
Collagen
GAG
Wall Area (× 10-2mm2)
0d
4d
14d
28d
E
Adv
Med
Neo
224d
B
DTA
F
C
SAA
G
D
IAA
H
I
Adventitia
Media
Neointima
Area Fraction (%)
Adventitia Media Neointima
J
K
L

Figure S5. (A-D) Extracellular matrix composition – elastin, smooth muscle cells (SMC), collagen, and glycosaminoglycans (GAG) – quantified as a fraction of overall aortic cross-sectional area in the ATA, DTA, SAA, and IAA after 0, 4, 14, and 28 days of AngII infusion (cf. Figure 2B-E in the main text). The dashed line demarcates relative areas of the media (below) and adventitia (above). (E-H) Layer-specific cross-sectional areas – neointimal (Neo), medial (Med), and adventitial (Adv) – at baseline (0 day), 28 and 224 days post-surgery. Note the regional variation in neointimal development at 224 days, with development most pronounced in the IAA (cf. Figure 5I-P in the main text). (I-L) Representative images illustrating semi-automated layer separation and cross-sectional area quantification in 224 day, VVG-stained, samples. All non-background pixels were counted, and data are presented as relative area fractions of each layer. Scale bar represents 250 μm. Tables S4 and S5 contain all tabulated values.

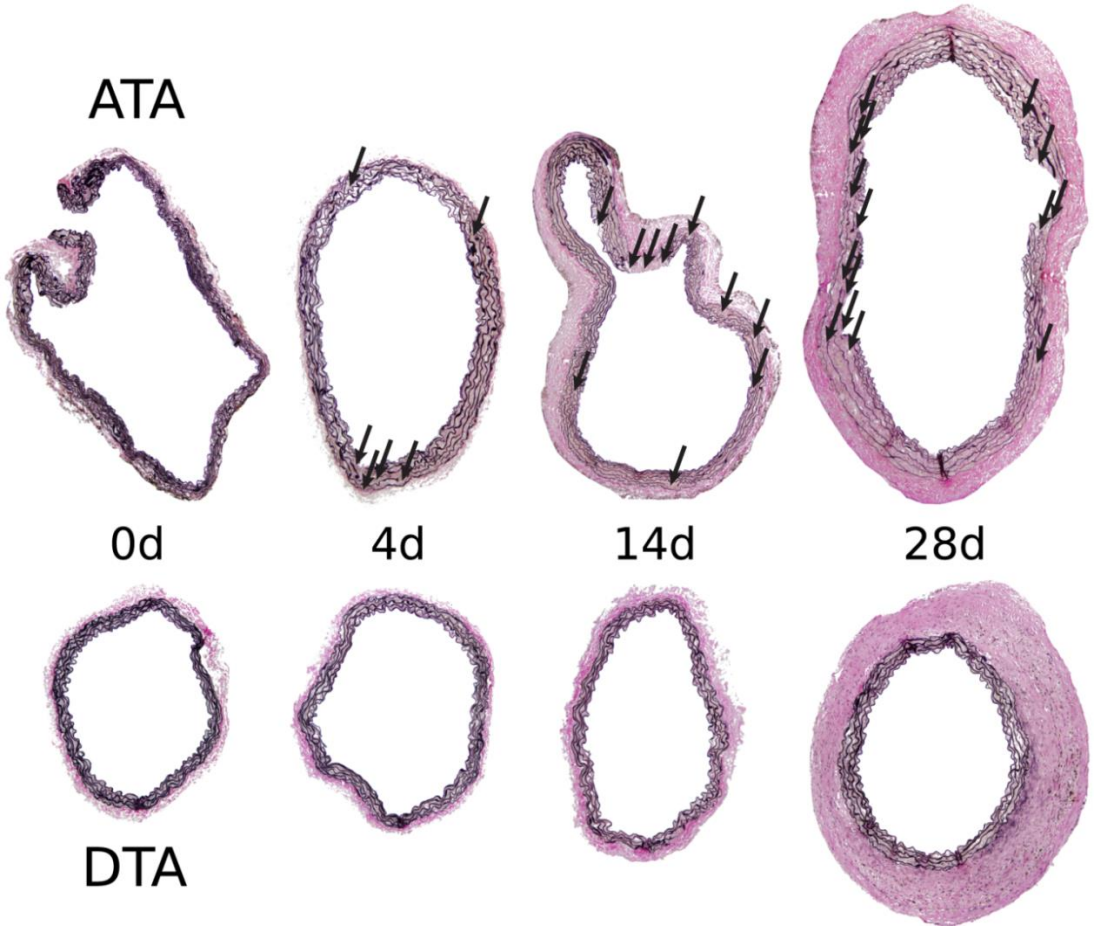

Figure S6. Representative histological cross-sections from VVG staining from the ascending (ATA) and descending (DTA) thoracic aorta at four times of AngII infusion: baseline (0 days), 4, 14, and 28 days. Elastin laminae are stained black and locations of elastin breakage are denoted by black arrows. Note the increasing number of breaks in the ATA with increasing duration of AngII infusion but the lack of breaks in the DTA. Indeed, the ATA was the only region with significant elastin breakage throughout AngII infusion and the only region with a propensity toward aneurysmal dilatation. Images are not to scale but are sized to highlight locations of elastin breakage.

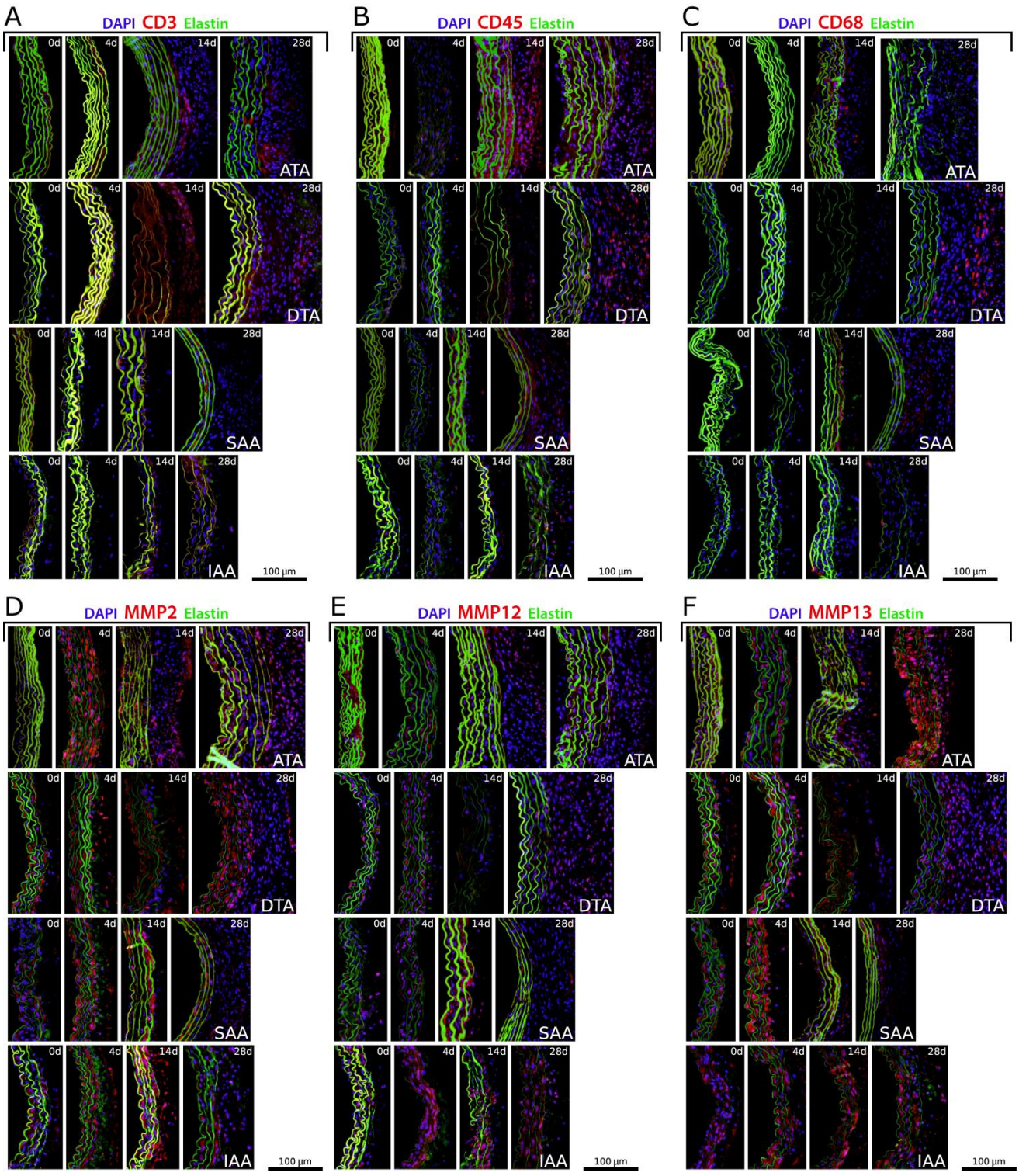

Figure S7. Representative immunofluorescence staining for each of the four aortic regions (ATA, DTA, SAA, and IAA) at four times of AngII infusion: baseline (0 days), 4, 14, and 28 days. Shown are sections of merged cross-sectional images containing cell nuclei in blue (DAPI), elastin in green (auto-fluorescent), and in red either (A-C) inflammatory cells (CD3 – T-cell, CD45 – pan inflammatory leukocyte marker, CD68 – macrophage) or (D-F) MMPs (-2, -12, -13). Quantification of immunofluorescence images can be found in Figure 3 in the main text. Scale bar represents 100 µm.

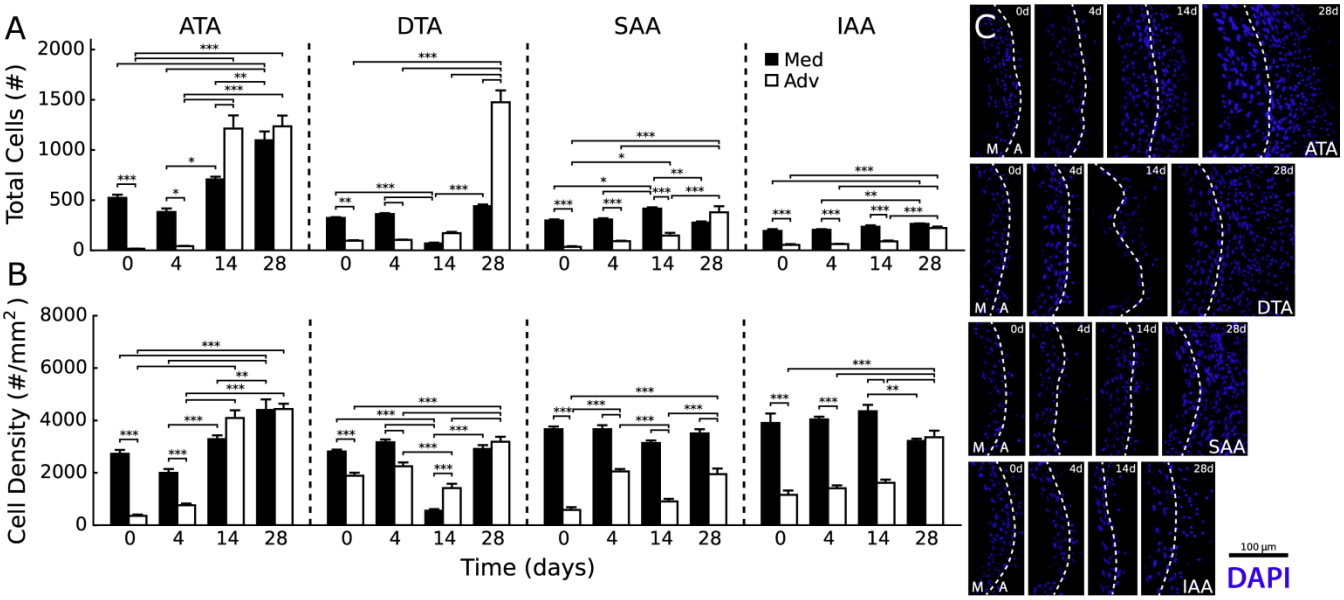

Figure S8. Quantification of (A) total cell nuclei and (B) cell density in the four regions (ATA, DTA, SAA, and IAA) as a function of the two primary layers of the aortic wall (media, black and adventitia, white) at four times of AngII infusion: baseline (0 days), 4, 14, and 28 days. (C) Images from the blue DAPI channel were analyzed to determine the number of non-connected cell nuclei. Note that medial cell number increased most notably in the ATA (likely SMC hyperplasia) whereas increased SMC mass in other regions is likely due to hypertrophy[28]. Bars denote statistical significance between groups, where *, **, *** $p < 0.05$, 0.01, 0.001. Scale bar represents 100 μm. Data are summarized in Tables S5A-D.

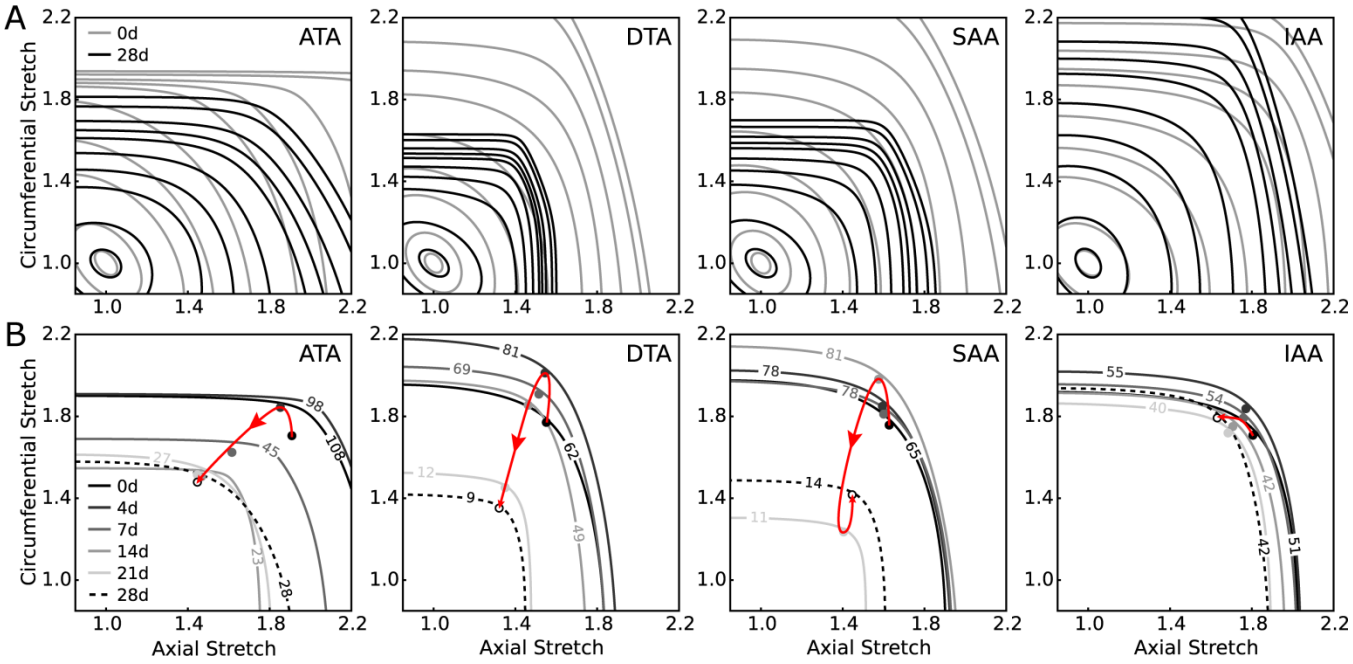

Figure S9. (A). Iso-energy contour plots showing predicted values of the energy storage function *W*, based on the identified set of best-fit material parameters (Table S3), at multiple combinations of circumferential and axial stretch for each of the four tested regions (ATA, DTA, SAA, and IAA) at 0 (grey) and 28 days (black) of AngII infusion. (B) Evolution of the *in vivo* energy contours based on the identified values of *in vivo* biaxial stretch and systolic blood pressures at baseline (0 days), 4, 7, 14, 21, and 28 days of AngII infusion. Red arrows show the trajectory of the *in vivo* biaxial stretch during AngII infusion; note the reduction in all regions except the IAA.

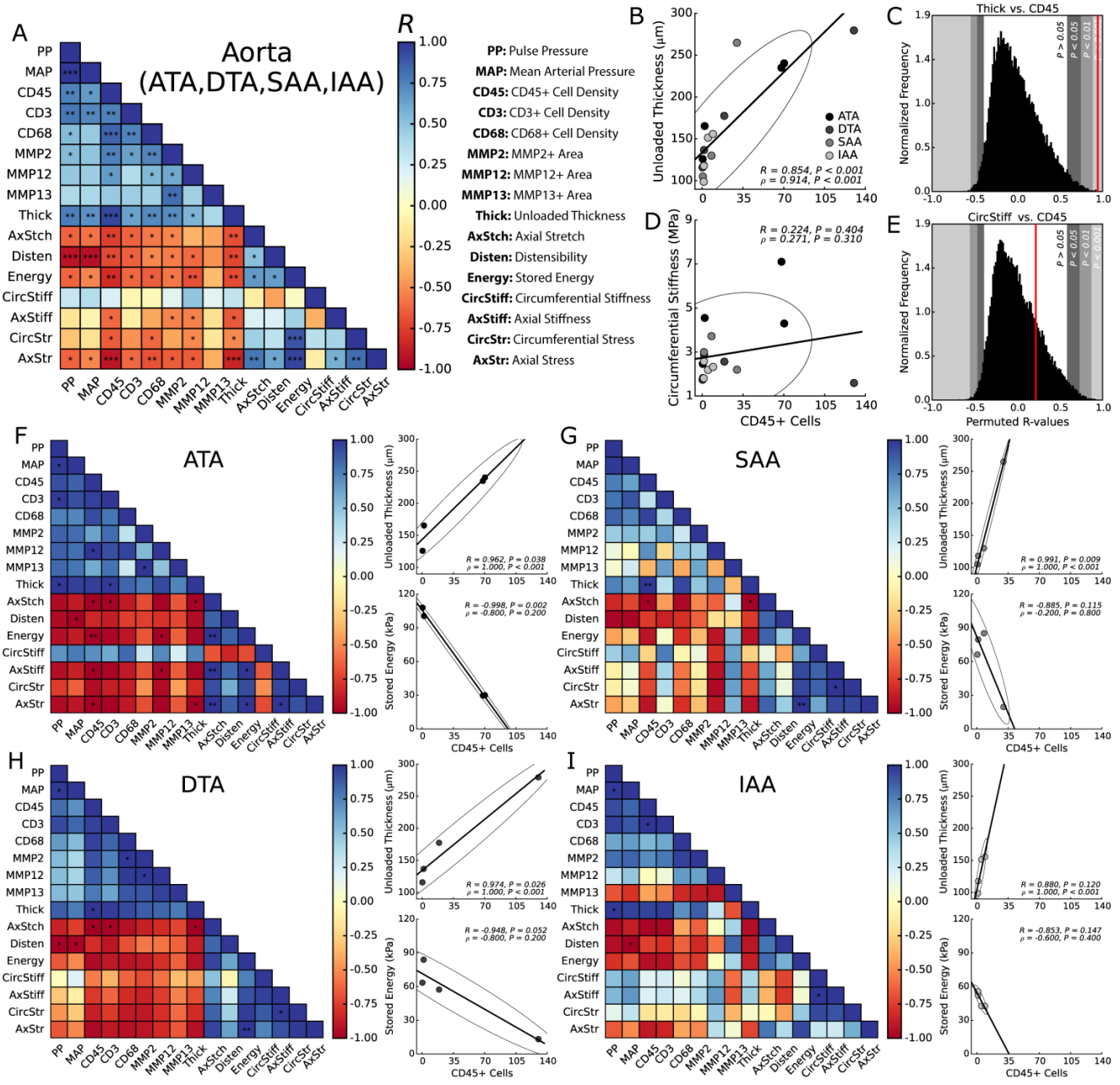

Figure S10. (A) Lower diagonal matrices of Pearson correlation coefficients ($R \in [-1,1]$) between mechanical and inflammatory metrics pooled from all four regions (n = 16 points total). (B) Illustrative strong positive correlation between wall thickness and CD45$^+$ cells and (C) the associated histogram of permuted R-values used to determine statistical significance (Red line; $p < 0.001$). (D) Illustrative weak correlation between circumferential stiffness and CD45$^+$ cells and (E) the associated R-value histogram with a non-significant correlation (Red line; $p > 0.05$). (F-I) Lower diagonal correlation matrices from individual regions (n = 4 points each) with illustrative positive (e.g., thickness vs. CD45$^+$ cells) and negative (e.g., stored energy vs. CD45$^+$ cells) correlations shown; individual plots include Pearson and Spearman correlation coefficients, p-values, and 95% confidence ellipses. For all correlation matrices, blue indicates a positive correlation and red indicates a negative correlation. All correlation coefficients and associated p-values can be found in Tables S6A-N. *, **, *** $p < 0.05$, 0.01, 0.001.

Supplemental Tables

Table S1 – Time course of measured blood pressures (diastolic, mean, systolic, and pulse) from 0 to 28 days of AngII infusion as well as at 224 days after pump implantation (with 7-months of no AngII infusion) relative to age-matched controls at days 0 and 224. Note that pressures tend to reach steady state values by 14 days. The systolic ratio measures the fold-change in systolic pressure relative to day 0, and can be used as a comparative target for geometric adaptation[17]. *** $p < 0.001$ vs. 0d, $^{\#}$ $p < 0.05$ vs. 28d, †, ††, ††† $p < 0.05$, 0.01, 0.001 vs. 224d no AngII.

	AngII Infusion Time							
	0d	4d	7d	14d	21d	28d	224d	224d no AngII
n	18	18	19	14	10	11	3	6
Blood Pressure (mmHg)								
Systolic	111.6 ± 4.1	155.4 ± 8.1 ***,#	167.6 ± 6.6 ***	181.3 ± 5.0 ***,††	183.9 ± 4.1 ***,††	186.2 ± 6.1 ***,††	140.4 ± 10.7	138.0 ± 5.3
Mean	90.2 ± 3.5	130.2 ± 7.6 ***	140.2 ± 6.0 ***	152.3 ± 4.8 ***,†	154.2 ± 3.7 ***,†	155.7 ± 5.7 ***,†	117.5 ± 10.2	116.0 ± 5.5
Diastolic	80.0 ± 3.3	118.0 ± 7.4 ***	127.1 ± 5.6 ***	138.3 ± 4.7 ***,†	139.9 ± 3.6 ***,†	140.9 ± 5.5 ***,†	106.5 ± 10.0	105.4 ± 5.6
Pulse Pressure	31.7 ± 1.6	37.4 ± 1.6 #	40.5 ± 1.5 ***	43.0 ± 1.0 ***,††	44.0 ± 1.4 ***,††	45.3 ± 1.5 ***,†††	33.9 ± 2.7	32.6 ± 1.3
Systolic Ratio	1.00	1.39	1.50	1.62	1.65	1.67	1.26	1.24

Table S2A – Morphological and mechanical data (mean ± SEM) for the ascending thoracic aorta (**ATA)** at multiple times from 0 to 28 days of AngII infusion as well as at 224 days after pump implantation (with 7-months of no AngII infusion) relative to age-matched controls at days 0 and 224. Pressure-dependent values were calculated at group-specific *systolic* pressures. $^{+}p < 0.1$, $^{*}p < 0.05$, $^{**}p < 0.01$, $^{***}p < 0.001$ vs. 0d

	ATA							
	0d	4d	7d	14d	21d	28d	224d	224d no AngII
n	5	5	5	6	6	7	3	5
Unloaded Dimensions								
Outer Diameter (μm)	1252 ± 36	1280 ± 39	1411 ± 61	1634 ± 77 *	1641 ± 67 **	1748 ± 92 **	1690 ± 100 ***	1399 ± 31
Wall Thickness (μm)	126 ± 3	165 ± 4	196 ± 23 +	235 ± 12 ***	237 ± 20 ***	240 ± 16 ***	218 ± 36 *	149 ± 4
In-vitro Axial Length (mm)	2.6 ± 0.1	2.8 ± 0.1	2.7 ± 0.1	3.2 ± 0.1 *	3.1 ± 0.1	3.2 ± 0.1 *	3.4 ± 0.1 *	3.0 ± 0.2
Systolic Dimensions								
Outer Diameter (μm)	1958 ± 42	2109 ± 41	2098 ± 36	2236 ± 58 *	2231 ± 43 *	2332 ± 65 ***	2495 ± 94 ***	2142 ± 54
Inner Radius (μm)	940 ± 21	1006 ± 22	978 ± 23	1010 ± 32	1004 ± 20	1052 ± 27 +	1149 ± 29 ***	1018 ± 27
Wall Thickness (μm)	39 ± 1	48 ± 3	72 ± 11	108 ± 12 **	111 ± 13 ***	115 ± 12 ***	98 ± 20 *	52 ± 2
In-vivo Axial Stretch	1.91 ± 0.01	1.86 ± 0.06	1.68 ± 0.07 +	1.47 ± 0.05 ***	1.45 ± 0.05 ***	1.44 ± 0.05 ***	1.39 ± 0.04 ***	1.70 ± 0.02 +
Systolic Cauchy Stresses (kPa)								
Circumferential	364.5 ± 11.0	435.7 ± 28.6	348.0 ± 67.4	243.9 ± 34.2	246.9 ± 45.5	239.4 ± 22.2	235.2 ± 41.3	359.7 ± 17.8
Axial	382.6 ± 6.8	341.2 ± 31.8	232.9 ± 58.2 *	123.7 ± 24.3 ***	125.2 ± 31.1 ***	122.3 ± 19.2 ***	142.0 ± 34.5 ***	295.9 ± 18.0
Systolic Stiffness (MPa)								
Circumferential	2.46 ± 0.22	4.55 ± 0.95	4.53 ± 1.71	7.10 ± 1.79	4.89 ± 1.20	4.30 ± 0.89	5.62 ± 1.08	4.81 ± 0.83
Axial	2.13 ± 0.06	2.05 ± 0.23	1.46 ± 0.36	0.97 ± 0.13 **	0.98 ± 0.24 **	0.90 ± 0.12 **	0.86 ± 0.16 *	1.86 ± 0.14
Systolic Structural Stiffness (N/m)	94.8 ± 8.4	226.9 ± 61.1	303.4 ± 111.0	763.0 ± 236.0 *	564.5 ± 177.9	496.6 ± 113.7	507.3 ± 17.3	254.4 ± 47.9
Systolic Stored Energy (kPa)	108.0 ± 3.4	100.5 ± 11.4	68.8 ± 21.7	29.7 ± 7.5 ***	31.6 ± 9.4 ***	30.0 ± 5.9 ***	32.7 ± 9.1 **	80.3 ± 5.8
Distensibility (MPa^{-1})	21.4 ± 2.2	9.6 ± 1.4 ***	8.2 ± 2.0 ***	3.3 ± 0.8 ***	4.6 ± 1.1 ***	4.8 ± 1.1 ***	4.7 ± 0.3 ***	8.9 ± 1.5 ***

Table S2B – Morphological and mechanical data (mean ± SEM) for the proximal descending thoracic aorta (**DTA)** at multiple times from 0 to 28 days of AngII infusion as well as at 224 days after pump implantation (with 7-months of no AngII infusion) relative to age-matched controls at days 0 and 224. Pressure-dependent values were calculated at group-specific *systolic* pressures. $^{+}p < 0.1$, $^{*}p < 0.05$, $^{**}p < 0.01$, $^{***}p < 0.001$ vs. 0d.

	DTA							
	0d	4d	7d	14d	21d	28d	224d	224d no AngII
n	5	7	5	5	5	5	3	5
Unloaded Dimensions								
Outer Diameter (μm)	943 ± 24	947 ± 23	1010 ± 20	995 ± 31 ***	1211 ± 33 **	1160 ± 67	1103 ± 82	953 ± 19
Wall Thickness (μm)	116 ± 5	137 ± 3	145 ± 8	177 ± 21	278 ± 18 ***	279 ± 26 ***	232 ± 44 **	128 ± 4
In-vitro Axial Length (mm)	5.2 ± 0.2	5.4 ± 0.2	5.2 ± 0.6	4.8 ± 0.4	5.7 ± 0.4	6.5 ± 0.2	5.7 ± 0.4	5.5 ± 0.2
Systolic Dimensions								
Outer Diameter (μm)	1505 ± 28	1683 ± 26 +	1709 ± 47 +	1593 ± 48	1508 ± 47	1353 ± 75	1494 ± 15	1518 ± 42
Inner Radius (μm)	710 ± 13	797 ± 12	805 ± 26	729 ± 35	612 ± 32	514 ± 53 **	632 ± 36	711 ± 22
Wall Thickness (μm)	42 ± 1	44 ± 2	50 ± 3	68 ± 14	142 ± 13 ***	162 ± 23 ***	115 ± 30 *	48 ± 2
In-vivo Axial Stretch	1.55 ± 0.01	1.54 ± 0.02	1.51 ± 0.02	1.46 ± 0.04	1.35 ± 0.04 ***	1.32 ± 0.03 ***	1.32 ± 0.01 ***	1.51 ± 0.02
Systolic Cauchy Stresses (kPa)								
Circumferential	252.7 ± 4.7	378.2 ± 10.7 *	371.2 ± 36.8 +	295.0 ± 45.5	110.8 ± 13.8 *	96.9 ± 34.0 **	119.8 ± 32.3 +	276.8 ± 20.8
Axial	237.2 ± 5.6	295.8 ± 12.1	262.0 ± 22.0	218.2 ± 35.9	81.1 ± 12.0 ***	72.8 ± 22.5 ***	92.2 ± 26.2 **	243.9 ± 14.9
Systolic Stiffness (MPa)								
Circumferential	1.74 ± 0.08	2.87 ± 0.10 **	3.10 ± 0.30 **	2.56 ± 0.26 +	1.67 ± 0.12	1.59 ± 0.20	1.09 ± 0.11	2.16 ± 0.16
Axial	2.91 ± 0.13	4.64 ± 0.33 **	3.94 ± 0.19	3.90 ± 0.57	2.01 ± 0.25	1.69 ± 0.38	1.46 ± 0.28	3.91 ± 0.22
Systolic Structural Stiffness (N/m)	73.0 ± 3.4	125.6 ± 5.6	151.3 ± 8.2 +	161.1 ± 11.8 *	232.7 ± 14.9 ***	252.4 ± 45.4 ***	118.6 ± 18.0	102.3 ± 3.0
Systolic Stored Energy (kPa)	63.4 ± 0.7	83.9 ± 3.3	72.2 ± 7.3	57.3 ± 10.7	13.8 ± 2.2 ***	13.2 ± 7.2 ***	20.9 ± 7.0 **	60.1 ± 5.6
Distensibility (MPa^{-1})	20.7 ± 1.0	12.3 ± 0.6 ***	9.8 ± 0.7 ***	8.6 ± 0.9 ***	4.9 ± 0.4 ***	4.7 ± 1.2 ***	11.4 ± 2.1 ***	13.1 ± 0.5 ***

Table S2C – Morphological and mechanical data (mean ± SEM) for the suprarenal abdominal aorta (**SAA)** at multiple times from 0 to 28 days of AngII infusion. Data were not collected at 224 days post-surgery since the long-term mice had pre-existing SAA dissections. Pressure-dependent values were calculated at group-specific *systolic* pressures. $^{+}p < 0.1$, $^{*}p < 0.05$, $^{**}p < 0.01$, $^{***}p < 0.001$ vs. 0d.

	SAA							
	0d	4d	7d	14d	21d	28d	224d	224d no AngII
n	6	6	4	4	4	4	-	-
Unloaded Dimensions								
Outer Diameter (μm)	838 ± 18	907 ± 7	947 ± 59	879 ± 67	1323 ± 84 ***	1247 ± 62 ***	-	-
Wall Thickness (μm)	105 ± 4	118 ± 3	120 ± 10	130 ± 16	238 ± 54 *	265 ± 45 **	-	-
In-vitro Axial Length (mm)	4.7 ± 0.3	6.0 ± 0.6	5.2 ± 1.1	4.8 ± 0.7	5.7 ± 0.3	6.2 ± 0.9	-	-
Systolic Dimensions								
Outer Diameter (μm)	1322 ± 16	1501 ± 37	1541 ± 39	1529 ± 117	1478 ± 95	1527 ± 93	-	-
Inner Radius (μm)	624 ± 9	710 ± 20	728 ± 26	723 ± 53	602 ± 75	627 ± 69	-	-
Wall Thickness (μm)	37 ± 2	40 ± 2	43 ± 8	42 ± 6	137 ± 29 **	137 ± 32 **	-	-
In-vivo Axial Stretch	1.63 ± 0.02	1.59 ± 0.02	1.60 ± 0.05	1.57 ± 0.06	1.40 ± 0.03 **	1.45 ± 0.04 *	-	-
Systolic Cauchy Stresses (kPa)								
Circumferential	255.8 ± 14.1	369.7 ± 24.2	421.0 ± 75.7 +	431.2 ± 34.7 +	140.8 ± 55.6	148.2 ± 53.2	-	-
Axial	267.8 ± 21.2	319.7 ± 12.3	333.8 ± 61.2	335.3 ± 46.7	103.6 ± 30.7 *	102.4 ± 36.5 *	-	-
Systolic Stiffness (MPa)								
Circumferential	1.82 ± 0.10	3.00 ± 0.15	3.51 ± 0.62 +	3.72 ± 0.22 *	3.00 ± 0.80	2.20 ± 0.61	-	-
Axial	2.57 ± 0.15	3.91 ± 0.18 +	3.62 ± 0.77	4.26 ± 0.16 *	1.63 ± 0.36	1.64 ± 0.55	-	-
Systolic Structural Stiffness (N/m)	66.5 ± 2.1	119.4 ± 1.4	135.9 ± 7.5	152.7 ± 13.5	356.9 ± 89.5 ***	249.5 ± 18.4 **	-	-
Systolic Stored Energy (kPa)	66.3 ± 4.9	79.6 ± 6.2	84.4 ± 18.2	85.2 ± 10.5	15.1 ± 7.3 **	19.6 ± 8.1 *	-	-
Distensibility (MPa^{-1})	19.1 ± 0.5	10.8 ± 0.3 ***	9.9 ± 0.7 ***	8.4 ± 0.2 ***	3.3 ± 0.6 ***	4.5 ± 0.3 ***	-	-

Table S2D – Morphological and mechanical data (mean ± SEM) for the infrarenal abdominal aorta (**IAA)** at multiple times from 0 to 28 days of AngII infusion as well as at 224 days after pump implantation (with 7-months of no AngII infusion) relative to age-matched controls at days 0 and 224. Pressure-dependent values were calculated at group-specific *systolic* pressures. $^{+}p < 0.1$, $^{*}p < 0.05$, $^{**}p < 0.01$, $^{***}p < 0.001$ vs. 0d.

	IAA							
	0d	4d	7d	14d	21d	28d	224d	224d no AngII
n	5	7	5	5	5	5	3	5
Unloaded Dimensions								
Outer Diameter (μm)	608 ± 18	634 ± 9	669 ± 15	682 ± 33	725 ± 17 *	702 ± 37	932 ± 68 ***	699 ± 14
Wall Thickness (μm)	99 ± 2	118 ± 3	128 ± 5 +	151 ± 8 ***	153 ± 10 ***	156 ± 12 ***	391 ± 9 ***	125 ± 4
In-vitro Axial Length (mm)	5.2 ± 0.7	5.4 ± 0.3	5.6 ± 0.2	5.3 ± 0.4	5.8 ± 0.5	6.3 ± 0.3	7.4 ± 0.8 +	5.9 ± 0.5
Systolic Dimensions								
Outer Diameter (μm)	898 ± 25	981 ± 23	1009 ± 28	973 ± 42	1035 ± 47	1033 ± 49	1089 ± 78 +	1017 ± 24
Inner Radius (μm)	417 ± 13	454 ± 12	464 ± 14	435 ± 18	464 ± 23	464 ± 24	350 ± 60	468 ± 13
Wall Thickness (μm)	32 ± 1	36 ± 1	41 ± 1	51 ± 4	53 ± 4	53 ± 3	194 ± 47 ***	41 ± 2
In-vivo Axial Stretch	1.81 ± 0.02	1.77 ± 0.04	1.76 ± 0.03	1.71 ± 0.04	1.69 ± 0.04	1.63 ± 0.02 +	1.30 ± 0.13 ***	1.80 ± 0.02
Systolic Cauchy Stresses (kPa)								
Circumferential	194.3 ± 9.8	259.2 ± 11.7 *	256.9 ± 10.7 *	207.6 ± 10.1	217.6 ± 17.9	221.0 ± 15.4	40.5 ± 14.0 ***	212.1 ± 13.2
Axial	256.7 ± 8.2	281.8 ± 12.2	278.8 ± 8.9	240.9 ± 19.4	234.0 ± 23.0	226.2 ± 13.2	53.6 ± 17.0 ***	252.0 ± 13.7
Systolic Stiffness (MPa)								
Circumferential	1.81 ± 0.10	2.58 ± 0.13 *	2.60 ± 0.14 *	2.19 ± 0.09	2.31 ± 0.22	2.32 ± 0.23	0.41 ± 0.10 ***	2.28 ± 0.14
Axial	2.93 ± 0.12	3.96 ± 0.18	4.27 ± 0.18 +	3.53 ± 0.27	4.02 ± 0.52	3.61 ± 0.45	0.94 ± 0.21 **	4.02 ± 0.12
Systolic Structural Stiffness (N/m)	58.0 ± 2.6	93.6 ± 4.2 *	105.5 ± 5.5 **	111.6 ± 8.2 ***	121.1 ± 9.7 ***	120.7 ± 9.5 ***	72.6 ± 14.4	93.0 ± 6.1 *
Systolic Stored Energy (kPa)	52.0 ± 1.8	55.8 ± 3.1	54.4 ± 2.1	42.6 ± 3.8	42.5 ± 3.9	42.7 ± 1.8	7.9 ± 4.3 ***	46.2 ± 3.8
Distensibility (MPa^{-1})	13.5 ± 0.8	8.5 ± 0.5 ***	7.7 ± 0.4 ***	6.9 ± 0.4 ***	6.8 ± 0.3 ***	6.9 ± 0.6 ***	13.3 ± 2.0	8.7 ± 0.9 ***

Table S3 – Best-fit values of the model parameters (Equation S1) used to characterize the mean (i.e., bulk or transmurally averaged) mechanical properties of the four aortic regions (ATA, DTA, SAA, IAA) at each experimental time of interest. Note that mechanical properties were not quantified in the SAA at 224 days due to prior aortic dissections, thus no age-matched controls were quantified at that time.

		Material Parameters								
		Elastic Fibers	Axial Collagen		Circ. Collagen + SMC		Diagonal Collagen			Error
		c (kPa)	c_1^1 (kPa)	c_2^1	c_1^2 (kPa)	c_2^2	$c_1^{3,4}$ (kPa)	$c_2^{3,4}$	α_0 (deg)	*RMSE*
ATA	0d	18.853	14.410	$2.34\text{X}10^{-14}$	16.556	0.100	5.120	0.313	48.609	0.079
	4d	15.591	10.562	$2.32\text{X}10^{-14}$	6.999	0.202	4.258	0.292	45.266	0.074
	7d	0.002	14.968	0.007	$3.52\text{X}10^{-5}$	4.904	19.323	0.226	55.862	0.106
	14d	1.794	6.093	0.461	$5.56\text{X}10^{-6}$	9.657	12.828	0.781	52.229	0.087
	21d	5.895	5.509	0.358	8.439	0.972	6.616	1.154	43.838	0.104
	28d	3.532	9.585	0.018	14.175	0.931	9.184	1.094	43.915	0.111
	224d	$7.99\text{X}10^{-9}$	15.459	0.270	$2.49\text{X}10^{-5}$	4.676	15.743	0.595	49.564	0.103
224d no AngII		29.955	4.338	0.225	0.008	2.262	7.997	0.459	50.538	0.051
DTA	0d	19.494	21.380	0.134	13.249	0.119	0.225	1.688	30.188	0.069
	4d	18.426	18.373	0.175	9.463	0.068	0.165	1.609	28.436	0.064
	7d	17.384	13.719	0.282	9.889	0.124	0.333	1.705	28.517	0.064
	14d	14.176	13.378	0.394	7.813	0.164	0.243	2.310	26.959	0.057
	21d	12.270	0.808	3.641	2.682	1.794	0.042	7.179	36.093	0.111
	28d	10.843	1.405	3.467	6.389	2.413	0.233	7.339	33.226	0.070
	224d	13.643	2.170	3.365	4.154	0.514	0.683	3.720	30.908	0.057
224d no AngII		20.127	17.417	0.288	10.600	0.186	0.117	2.432	27.497	0.061
SAA	0d	14.010	22.108	0.081	15.514	0.100	0.545	1.079	33.931	0.069
	4d	17.167	19.968	0.109	13.399	0.118	0.538	1.214	31.919	0.053
	7d	20.035	10.931	0.223	13.210	0.162	0.953	1.090	32.917	0.056
	14d	15.782	17.653	0.102	9.162	0.101	0.463	1.206	30.317	0.053
	21d	15.546	0.128	3.969	11.152	6.253	0.584	7.321	46.172	0.086
	28d	8.516	3.419	1.058	7.259	1.729	0.266	3.532	35.884	0.065
	224d	-	-	-	-	-	-	-	-	-
224d no AngII		-	-	-	-	-	-	-	-	-
IAA	0d	10.646	7.838	0.130	8.809	0.235	0.217	0.865	35.372	0.080
	4d	8.800	8.658	0.130	7.957	0.168	0.143	0.949	33.459	0.079
	7d	8.738	10.967	0.099	9.030	0.207	0.059	1.213	31.987	0.062
	14d	7.919	8.209	0.152	6.883	0.261	0.250	1.068	33.116	0.072
	21d	11.671	3.410	0.409	6.426	0.329	0.094	1.474	32.540	0.081
	28d	7.765	12.921	0.129	6.715	0.234	0.094	1.592	28.887	0.055
	224d	1.085	11.606	1.735	2.425	0.247	0.048	6.165	26.148	0.081
224d no AngII		8.069	9.225	0.073	9.690	0.272	0.035	1.272	33.489	0.082

Table S4 – Quantification of layer-specific cross-sectional area and wall percentage as measured from histological images. Relative amounts of media, adventitia, and neointima are delineated for each of the four regions at five experimental times during AngII infusion. Graphical representations can be found in Figures 2 and 5 in the main text, and representative images of layer segmentation can be found in Figure S5. $^{**}p < 0.01$, $^{***}p < 0.001$ vs. 0d in a given layer, $^{\dagger\dagger\dagger}p < 0.001$ between layers at a given time.

		AngII Infusion Time				
		0d	4d	14d	28d	224d
ATA	Cross-sectional Area (mm^2)					
	Media	0.348 ± 0.008	0.383 ± 0.011	0.448 ± 0.032 ***	0.515 ± 0.021 ***	0.705 ± 0.024 ***
	Adventitia	0.097 ± 0.008 †††	0.125 ± 0.011 †††	0.514 ± 0.033 ***	0.536 ± 0.021 ***	0.309 ± 0.027 †††,***
	Neointima	-	-	-	-	0.129 ± 0.008
	Wall Percentage (%)					
	Media	78.3 ± 1.8	75.3 ± 2.1	46.6 ± 3.4	49.1 ± 1.9	61.7 ± 2.2
	Adventitia	21.8 ± 1.8	24.7 ± 2.1	53.6 ± 3.4	51.1 ± 1.9	27.0 ± 2.4
	Neointima	-	-	-	-	11.3 ± 0.7
DTA	Cross-sectional Area (mm^2)					
	Media	0.209 ± 0.005	0.229 ± 0.005	0.230 ± 0.019	0.245 ± 0.014	0.298 ± 0.018 ***
	Adventitia	0.094 ± 0.005 †††	0.099 ± 0.005 †††	0.270 ± 0.019 ***	0.687 ± 0.015 †††,***	0.266 ± 0.023 ***
	Neointima	-	-	-	-	0.022 ± 0.009
	Wall Percentage (%)					
	Media	69.0 ± 1.4	69.9 ± 1.1	45.2 ± 3.7	26.4 ± 1.6	50.9 ± 3.0
	Adventitia	31.0 ± 1.4	30.1 ± 1.1	54.8 ± 3.7	73.8 ± 1.7	45.4 ± 4.2
	Neointima	-	-	-	-	3.7 ± 1.4
SAA	Cross-sectional Area (mm^2)					
	Media	0.148 ± 0.005	0.175 ± 0.008	0.208 ± 0.019	0.257 ± 0.044	0.317 ± 0.009 **
	Adventitia	0.099 ± 0.005	0.090 ± 0.008	0.225 ± 0.019	0.369 ± 0.043 ***	3.745 ± 0.117 †††,***
	Neointima	-	-	-	-	0.061 ± 0.020
	Wall Percentage (%)					
	Media	60.0 ± 1.3	66.0 ± 1.7	48.7 ± 4.5	41.4 ± 7.3	7.7 ± 0.1
	Adventitia	40.0 ± 1.3	34.0 ± 1.7	51.3 ± 4.5	59.5 ± 7.2	90.9 ± 0.3
	Neointima	-	-	-	-	1.4 ± 0.4
IAA	Cross-sectional Area (mm^2)					
	Media	0.086 ± 0.005	0.097 ± 0.005	0.112 ± 0.003 ***	0.149 ± 0.003 ***	0.132 ± 0.006 ***
	Adventitia	0.083 ± 0.005	0.089 ± 0.005	0.113 ± 0.003 ***	0.121 ± 0.003 †††,***	0.180 ± 0.01 †††,***
	Neointima	-	-	-	-	0.416 ± 0.014
	Wall Percentage (%)					
	Media	50.7 ± 1.6	52.1 ± 2.5	49.9 ± 1.0	55.1 ± 1.0	18.1 ± 0.8
	Adventitia	48.6 ± 1.6	47.9 ± 2.5	50.5 ± 1.0	44.9 ± 1.0	24.7 ± 1.1
	Neointima	-	-	-	-	57.2 ± 1.8

Table S5A – Quantification of layer-specific (medial vs. adventitial) content of matrix constituents, inflammatory cell composition, and matrix metalloproteinases (MMPs) in the **ATA** at four times during AngII infusion. *, **, $^{***}p < 0.05, 0.01, 0.001$ vs. 0d in a given layer, †, ††, †††$p < 0.05, 0.01, 0.001$ between layers at a given time.

	ATA							
	Media				Adventitia			
	0d	4d	14d	28d	0d	4d	14d	28d
Area Fractions (%)								
Elastin	38.28 ± 1.97	27.64 ± 2.63	17.08 ± 1.04	19.30 ± 2.35	2.85 ± 0.51	0.15 ± 0.06	0.50 ± 0.07	0.55 ± 0.12
SMC	34.07 ± 1.90	46.40 ± 4.23	62.75 ± 1.72	61.11 ± 2.96	-	-	-	-
Collagen	23.49 ± 0.59	22.86 ± 0.25	18.43 ± 0.42	17.83 ± 0.12	97.15 ± 3.54	99.85 ± 1.32	99.50 ± 1.75	99.45 ± 2.27
GAG	4.16 ± 0.23	3.10 ± 0.25	1.74 ± 0.19	1.76 ± 0.25	-	-	-	-
Cell Nuclei Count (#)	523 ± 31	382 ± 36	707 ± 27	1097 ± 88 ***	16 ± 2 †††	42 ± 3 †	1212 ± 132 †††,***	1235 ± 107 ***
Cell Nuclei Density (#/mm^2)	2730 ± 145	2001 ± 146	3287 ± 144	4401 ± 402 ***	356 ± 52 †††	762 ± 67 †††	4095 ± 290 ***	4436 ± 201 ***
Inflammatory Cell Count (#)								
CD3	0.2 ± 0.2	1.5 ± 0.4	2.3 ± 0.6	8.2 ± 3.3	0.0 ± 0.0	1.5 ± 0.5	18.2 ± 8.5 *	20.7 ± 3.9 **
CD45	0.0 ± 0.0	1.3 ± 0.3	4.8 ± 0.8	16.7 ± 3.2	0.5 ± 0.3	0.8 ± 0.4	63.2 ± 22.2 ††,***	53.7 ± 13.8 **
CD68	0.3 ± 0.2	0.2 ± 0.2	5.8 ± 1.4	7.2 ± 3.0	0.3 ± 0.2	0.2 ± 0.2	18.3 ± 5.8 †,***	6.8 ± 2.3
Inflammatory Cell Density (#/mm^2)								
CD3	0.9 ± 0.9	9.6 ± 3.2	10.4 ± 2.7	49.1 ± 21.6	0.0 ± 0.0	24.9 ± 7.6	61.5 ± 22.2 *	76.7 ± 7.5 ***
CD45	0.0 ± 0.0	8.0 ± 2.2	22.9 ± 4.2	71.8 ± 15.8	12.1 ± 8.3	13.1 ± 6.3	200.2 ± 55.3 †††,***	185.6 ± 23.5 †,***
CD68	1.8 ± 1.1	1.1 ± 1.1	25.9 ± 5.5	37.5 ± 19.5	5.1 ± 3.2	3.3 ± 3.3	60.2 ± 13.4 **	22.7 ± 5.9
MMP Area Fraction (%)								
MMP2	1.47 ± 0.25	10.75 ± 2.18 *	2.18 ± 0.81	11.55 ± 4.15 **	0.14 ± 0.04	2.00 ± 0.44 †	3.76 ± 1.28	5.44 ± 0.67
MMP12	0.51 ± 0.09	0.40 ± 0.11	1.53 ± 0.51	0.46 ± 0.10	0.61 ± 0.23	0.24 ± 0.05	1.80 ± 0.84	1.84 ± 0.79
MMP13	0.95 ± 0.18	9.03 ± 2.36	3.15 ± 0.88	12.08 ± 4.99 *	0.58 ± 0.14	1.93 ± 0.59	2.06 ± 0.33	5.35 ± 2.39
Relative MMP Expression								
MMP2	1.0 ± 0.2	7.3 ± 1.5	1.5 ± 0.5	7.9 ± 2.8	1.0 ± 0.3	14.7 ± 3.2	27.6 ± 9.4 ††,**	40.0 ± 4.9 †††,***
MMP12	1.0 ± 0.2	0.8 ± 0.2	3.0 ± 1.0	0.9 ± 0.2	1.0 ± 0.4	0.4 ± 0.1	3.0 ± 1.4	3.0 ± 1.3
MMP13	1.0 ± 0.2	9.5 ± 2.5	3.3 ± 0.9	12.7 ± 5.2 *	1.0 ± 0.2	3.3 ± 1.0	3.5 ± 0.6	9.2 ± 4.1

Table S5B – Quantification of layer-specific (medial vs. adventitial) content of matrix constituents, inflammatory cell composition, and matrix metalloproteinases (MMPs) in the **DTA** at four time points during AngII infusion. *, **, $^{***}p < 0.05, 0.01, 0.001$ vs. 0d in a given layer, †, ††, ††† $p < 0.05, 0.01, 0.001$ between layers at a given time.

	DTA							
	Media				Adventitia			
	0d	4d	14d	28d	0d	4d	14d	28d
Area Fractions (%)								
Elastin	32.95 ± 1.87	28.57 ± 1.47	29.08 ± 2.40	27.83 ± 0.65	0.17 ± 0.04	0.22 ± 0.06	0.08 ± 0.04	0.23 ± 0.05
SMC	44.06 ± 2.66	44.82 ± 0.87	28.05 ± 1.63	51.02 ± 1.20	-	-	-	-
Collagen	18.62 ± 1.06	19.73 ± 0.55	35.96 ± 3.02	17.03 ± 0.19	99.83 ± 2.07	99.78 ± 2.55	99.92 ± 2.09	99.77 ± 2.84
GAG	4.36 ± 0.46	6.87 ± 0.75	6.91 ± 0.89	4.12 ± 1.25	-	-	-	-
Cell Nuclei Count (#)	323 ± 8	362 ± 9	69 ± 8 ***	441 ± 17	96 ± 5 ††	105 ± 3 †††	172 ± 12	1475 ± 118 †††,***
Cell Nuclei Density (#/mm^2)	2816 ± 73	3169 ± 102	556 ± 57 ***	2911 ± 146	1891 ± 114 †††	2250 ± 145 †††	1417 ± 164 †††	3189 ± 186 ***
Inflammatory Cell Count (#)								
CD3	0.3 ± 0.2	0.3 ± 0.3	3.3 ± 1.9	5.5 ± 2.2	0.8 ± 0.3	2.8 ± 1.4	19.2 ± 8.9	70.5 ± 28.1 ††,***
CD45	0.2 ± 0.2	0.5 ± 0.2	2.0 ± 1.4	11.8 ± 4.5	0.2 ± 0.2	1.2 ± 0.5	17.0 ± 9.0	118.3 ± 47.4 ††,***
CD68	0.0 ± 0.0	0.3 ± 0.2	0.0 ± 0.0	14.3 ± 7.5	0.0 ± 0.0	0.5 ± 0.2	0.3 ± 0.2	78.7 ± 29.6 ††,***
Inflammatory Cell Density (#/mm^2)								
CD3	2.8 ± 1.7	2.6 ± 2.6	24.4 ± 14.0	35.2 ± 12.8	17.1 ± 6.5	42.7 ± 21.1	75.2 ± 32.6	142.0 ± 53.4 *
CD45	1.4 ± 1.4	4.5 ± 2.1	14.6 ± 10.5	82.2 ± 32.5	3.5 ± 3.5	27.5 ± 13.4	74.1 ± 31.0	236.7 ± 90.4 **
CD68	0.0 ± 0.0	2.9 ± 1.9	0.0 ± 0.0	100.1 ± 53.1	0.0 ± 0.0	9.5 ± 4.6	2.7 ± 2.0	159.0 ± 55.6 **
MMP Area Fraction (%)								
MMP2	8.66 ± 0.74	7.58 ± 1.42	2.23 ± 0.98	15.43 ± 3.31	5.13 ± 0.52	4.56 ± 0.70	3.57 ± 1.83	3.68 ± 0.54 †††
MMP12	0.65 ± 0.16	1.12 ± 0.74	0.25 ± 0.13	0.74 ± 0.34	0.97 ± 0.19	0.74 ± 0.34	0.10 ± 0.06	0.93 ± 0.45
MMP13	7.48 ± 1.37	13.42 ± 1.79	6.60 ± 3.27	7.42 ± 1.03	3.09 ± 0.50	6.25 ± 0.91 †	1.36 ± 0.35	3.37 ± 0.77
Relative MMP Expression								
MMP2	1.0 ± 0.1	0.9 ± 0.2	0.3 ± 0.1	1.8 ± 0.4	1.0 ± 0.1	0.9 ± 0.1	0.7 ± 0.4	0.7 ± 0.1 †
MMP12	1.0 ± 0.2	1.7 ± 1.1	0.4 ± 0.2	1.1 ± 0.5	1.0 ± 0.2	0.8 ± 0.4	0.1 ± 0.1	1.0 ± 0.5
MMP13	1.0 ± 0.2	1.8 ± 0.2	0.9 ± 0.4	1.0 ± 0.1	1.0 ± 0.2	2.0 ± 0.3	0.4 ± 0.1	1.1 ± 0.2

Table S5C – Quantification of layer-specific (medial vs. adventitial) content of matrix constituents, inflammatory cell composition, and matrix metalloproteinases (MMPs) in the **SAA** at four time points during AngII infusion. *, **, $^{***}p < 0.05, 0.01, 0.001$ vs. 0d in a given layer, †, ††, ††† $p < 0.05, 0.01, 0.001$ between layers at a given time.

	SAA							
	Media				Adventitia			
	0d	4d	14d	28d	0d	4d	14d	28d
Area Fractions (%)								
Elastin	22.90 ± 1.77	22.04 ± 1.42	26.30 ± 2.00	34.40 ± 2.21	0.46 ± 0.14	0.14 ± 0.04	0.34 ± 0.05	0.96 ± 0.29
SMC	50.27 ± 2.03	48.28 ± 1.55	56.08 ± 2.22	43.71 ± 2.16	-	-	-	-
Collagen	21.66 ± 1.51	24.56 ± 1.45	14.97 ± 0.81	18.28 ± 0.19	99.54 ± 1.98	99.86 ± 4.92	99.66 ± 4.49	99.04 ± 2.44
GAG	5.17 ± 0.76	5.11 ± 0.56	2.64 ± 0.41	3.62 ± 0.28	-	-	-	-
Cell Nuclei Count (#)	298 ± 10	308 ± 12	417 ± 12 *	277 ± 11	35 ± 6 †††	92 ± 4 †††	147 ± 27 †††	380 ± 60 ***
Cell Nuclei Density (#/mm^2)	3664 ± 103	3667 ± 154	3141 ± 93	3506 ± 158	585 ± 100 †††	2057 ± 92 †††,***	907 ± 102 †††	1948 ± 218 †††,***
Inflammatory Cell Count (#)								
CD3	0.7 ± 0.3	1.5 ± 0.4	2.8 ± 0.7	3.0 ± 0.6	0.3 ± 0.2	2.7 ± 0.5	7.2 ± 1.6 †,***	3.8 ± 1.3
CD45	0.5 ± 0.2	1.0 ± 0.5	1.8 ± 0.4	4.0 ± 0.7	0.2 ± 0.2	0.5 ± 0.3	6.2 ± 2.7	25.8 ± 11.0 ††,**
CD68	0.2 ± 0.2	0.0 ± 0.0	2.0 ± 0.4	2.2 ± 0.3	0.0 ± 0.0	0.0 ± 0.0	2.3 ± 0.7	5.5 ± 2.3 **
Inflammatory Cell Density (#/mm^2)								
CD3	7.6 ± 3.6	18.2 ± 5.4	21.3 ± 5.2	43.8 ± 12.4 **	5.4 ± 3.4	59.0 ± 10.1 ††,***	43.1 ± 2.0 **	25.2 ± 4.5
CD45	5.9 ± 2.7	11.9 ± 5.9	13.9 ± 3.1	55.8 ± 15.8	2.7 ± 2.7	11.9 ± 8.2	25.6 ± 10.2	120.3 ± 44.6 ***
CD68	1.7 ± 1.7	0.0 ± 0.0	15.1 ± 2.7	29.5 ± 6.0 **	0.0 ± 0.0	0.0 ± 0.0	13.2 ± 3.2	25.5 ± 9.6 **
MMP Area Fraction (%)								
MMP2	3.03 ± 0.70	10.93 ± 2.96 **	3.55 ± 0.37	10.26 ± 1.98 *	3.16 ± 0.68	6.17 ± 1.20	0.85 ± 0.19	0.84 ± 0.26 †††
MMP12	1.81 ± 0.71	2.17 ± 1.02	0.81 ± 0.28	2.65 ± 0.71	1.03 ± 0.29	0.93 ± 0.38	0.34 ± 0.10	0.32 ± 0.18
MMP13	4.83 ± 1.40	22.98 ± 2.88 ***	5.36 ± 0.53	6.86 ± 1.03	0.64 ± 0.21	5.30 ± 0.75 †††	3.19 ± 0.54	0.42 ± 0.13 †
Relative MMP Expression								
MMP2	1.0 ± 0.2	3.6 ± 1.0 **	1.2 ± 0.1	3.4 ± 0.7 †††,*	1.0 ± 0.2	2.0 ± 0.4	0.3 ± 0.1	0.3 ± 0.1
MMP12	1.0 ± 0.4	1.2 ± 0.6	0.4 ± 0.2	1.5 ± 0.4	1.0 ± 0.3	0.9 ± 0.4	0.3 ± 0.1	0.3 ± 0.2
MMP13	1.0 ± 0.3	4.8 ± 0.6 **	1.1 ± 0.1	1.4 ± 0.2	1.0 ± 0.3	8.3 ± 1.2 ††,***	5.0 ± 0.8 †††,***	0.7 ± 0.2

Table S5D – Quantification of layer-specific (medial vs. adventitial) content of matrix constituents, inflammatory cell composition, and matrix metalloproteinases (MMPs) in the **IAA** at four time points during AngII infusion. *, **, $^{***}p< 0.05, 0.01, 0.001$ vs. 0d in a given layer, †, ††, ††† $p < 0.05, 0.01, 0.001$ between layers at a given time.

	IAA							
	Media				Adventitia			
	0d	4d	14d	28d	0d	4d	14d	28d
Area Fractions (%)								
Elastin	14.86 ± 1.97	18.30 ± 1.74	23.28 ± 1.64	15.54 ± 1.06	0.03 ± 0.01	0.07 ± 0.03	0.09 ± 0.02	0.14 ± 0.04
SMC	62.78 ± 2.86	63.74 ± 1.68	56.65 ± 2.02	64.06 ± 1.27	-	-	-	-
Collagen	18.80 ± 1.61	15.46 ± 0.96	17.27 ± 0.76	19.09 ± 0.13	99.97 ± 2.48	99.93 ± 5.30	99.91 ± 1.99	99.86 ± 3.74
GAG	3.56 ± 0.44	2.50 ± 0.25	2.80 ± 0.21	1.32 ± 0.16	-	-	-	-
Cell Nuclei Count (#)	193 ± 18	206 ± 6	235 ± 16	264 ± 6 ***	55 ± 8 †††	63 ± 4 †††	90 ± 8 †††	223 ± 15 ***
Cell Nuclei Density (#/mm^2)	3905 ± 361	4038 ± 104	4353 ± 243	3217 ± 87	1160 ± 165 †††	1412 ± 112 †††	1618 ± 124 †††	3360 ± 251 ***
Inflammatory Cell Count (#)								
CD3	0.0 ± 0.0	0.3 ± 0.2	4.7 ± 1.2 **	6.8 ± 1.4 ***	0.2 ± 0.2	0.8 ± 0.5	2.3 ± 1.1	5.8 ± 0.7 ***
CD45	0.7 ± 0.2	0.8 ± 0.3	2.5 ± 0.6	4.7 ± 1.2 **	0.7 ± 0.3	0.7 ± 0.3	2.5 ± 0.8	4.7 ± 0.7 **
CD68	0.3 ± 0.2	0.2 ± 0.2	3.2 ± 1.7	1.7 ± 0.9	0.0 ± 0.0	0.7 ± 0.3	1.5 ± 1.0	0.5 ± 0.3
Inflammatory Cell Density (#/mm^2)								
CD3	0.0 ± 0.0	6.6 ± 4.2	84.6 ± 20.3 *†	88.1 ± 22.0 **	3.6 ± 3.6	21.9 ± 14.3	40.4 ± 18.9	87.2 ± 10.9 **
CD45	13.5 ± 4.3	15.8 ± 5.7	47.3 ± 12.5	60.7 ± 16.6	14.2 ± 7.1	16.0 ± 8.6	45.4 ± 13.2	69.4 ± 10.6 *
CD68	6.7 ± 4.2	3.5 ± 3.5	55.3 ± 30.0	23.3 ± 12.8	0.0 ± 0.0	11.3 ± 5.6	25.6 ± 16.4	7.9 ± 5.4
MMP Area Fraction (%)								
MMP2	13.52 ± 2.21	15.04 ± 5.29	22.16 ± 4.54	10.60 ± 3.48	0.97 ± 0.24	4.80 ± 2.00	9.36 ± 2.19	5.74 ± 1.47
MMP12	4.87 ± 2.82	10.15 ± 4.63	8.44 ± 3.49	2.62 ± 1.16	0.46 ± 0.17	0.63 ± 0.19	1.55 ± 0.17	1.60 ± 0.37
MMP13	31.05 ± 3.16	21.74 ± 4.04	17.30 ± 4.49 *	15.54 ± 3.52 **	3.30 ± 1.06 †††	3.23 ± 0.6 †††	2.91 ± 0.71 †	2.86 ± 0.4.0 †
Relative MMP Expression								
MMP2	1.0 ± 0.2	1.1 ± 0.4	1.6 ± 0.3	0.8 ± 0.3	1.0 ± 0.3	4.9 ± 2.1	9.6 ± 2.3 †††,***	5.9 ± 1.5
MMP12	1.0 ± 0.6	2.1 ± 1.0	1.7 ± 0.7	0.5 ± 0.2	1.0 ± 0.4	1.4 ± 0.4	3.4 ± 0.4	3.5 ± 0.8 †
MMP13	1.0 ± 0.1	0.7 ± 0.1	0.6 ± 0.1	0.5 ± 0.1	1.0 ± 0.3	1.0 ± 0.2	0.9 ± 0.2	0.9 ± 0.1

Table S6A – Pearson correlation coefficients (*R*) for the pooled **Aorta** (ATA + DTA + SAA + IAA)

	PP	MAP	CD45	CD3	CD68	MMP2	MMP12	MMP13	Thick	AxStch	Disten	Energy	CircStiff	AxStiff	CircStr	AxStr
PP	1															
MAP	0.9792	1														
CD45	0.7463	0.6585	1													
CD3	0.7825	0.7304	0.7506	1												
CD68	0.5274	0.4622	0.8467	0.7471	1											
MMP2	0.5354	0.4879	0.7511	0.6378	0.7363	1										
MMP12	0.4750	0.4455	0.6637	0.3721	0.5454	0.6061	1									
MMP13	0.3871	0.3913	0.4683	0.4489	0.4363	0.8200	0.4347	1								
Thick	0.7606	0.6909	0.9446	0.6349	0.7220	0.7126	0.5593	0.3953	1							
AxStch	-0.6257	-0.5706	-0.7452	-0.6281	-0.5582	-0.5177	-0.3676	-0.4148	-0.6907	1						
Disten	-0.9080	-0.9267	-0.7162	-0.6403	-0.5101	-0.5453	-0.6065	-0.4834	-0.7197	0.5066	1					
Energy	-0.6219	-0.5209	-0.8198	-0.6168	-0.6471	-0.5609	-0.6910	-0.3370	-0.7062	0.6711	0.6486	1				
CircStiff	0.2899	0.3622	0.2165	-0.0520	-0.0275	0.1668	0.4804	0.1747	0.3063	-0.0964	-0.4309	0.0187	1			
AxStiff	-0.1660	-0.0589	-0.6131	-0.1038	-0.4170	-0.5306	-0.5350	-0.1826	-0.6665	0.2184	0.2064	0.4322	-0.3782	1		
CircStr	-0.3100	-0.1774	-0.6537	-0.4823	-0.6144	-0.4208	-0.5155	-0.1495	-0.5097	0.4408	0.3216	0.8992	0.3435	0.4110	1	
AxStr	-0.6259	-0.5217	-0.9034	-0.6114	-0.6828	-0.6491	-0.6562	-0.3839	-0.8445	0.7858	0.6215	0.9484	-0.0986	0.5815	0.8157	1

Legend

PP	Pulse Pressure	**Thick**	Unloaded Thickness
MAP	Mean Arterial Pressure	**AxStch**	Axial Stretch
CD45	CD45+ Cell Density	**Disten**	Distensibility
CD3	CD3+ Cell Density	**Energy**	Stored Energy
CD68	CD68+ Cell Density	**CircStiff**	Circumferential Stiffness
MMP2	MMP2+ Area	**AxStiff**	Axial Stiffness
MMP12	MMP12+ Area	**CircStr**	Circumferential Stress
MMP13	MMP13+ Area	**AxStr**	Axial Stress

Table S6B – Correlation *p*-values for the pooled **Aorta** (ATA + DTA + SAA + IAA)

	PP	MAP	CD45	CD3	CD68	MMP2	MMP12	MMP13	Thick	AxStch	Disten	Energy	CircStiff	AxStiff	CircStr	AxStr
PP	1															
MAP	0.000000	1														
CD45	0.000899	0.005540	1													
CD3	0.000340	0.001313	0.000807	1												
CD68	0.035769	0.071457	0.000035	0.000881	1											
MMP2	0.032581	0.055200	0.000798	0.007850	0.001144	1										
MMP12	0.062974	0.083719	0.005057	0.155820	0.028871	0.012820	1									
MMP13	0.138576	0.133977	0.067323	0.081139	0.091094	0.000100	0.092429	1								
Thick	0.000624	0.003042	0.000000	0.008231	0.001587	0.001949	0.024280	0.129626	1							
AxStch	0.009528	0.020983	0.000923	0.009175	0.024620	0.039975	0.161274	0.110126	0.003054	1						
Disten	0.000001	0.000000	0.001802	0.007545	0.043495	0.028924	0.012744	0.057858	0.001672	0.045219	1					
Energy	0.010105	0.038571	0.000101	0.010932	0.006742	0.023801	0.003032	0.201885	0.002231	0.004424	0.006565	1				
CircStiff	0.276133	0.167979	0.420618	0.848430	0.919402	0.536837	0.059635	0.517445	0.248586	0.722447	0.095677	0.945089	1			
AxStiff	0.538844	0.828520	0.011551	0.702056	0.108115	0.034482	0.032746	0.498404	0.004813	0.416505	0.443119	0.094530	0.148637	1		
CircStr	0.242568	0.510936	0.006019	0.058477	0.011325	0.104576	0.040989	0.580570	0.043715	0.087480	0.224436	0.000002	0.192741	0.113757	1	
AxStr	0.009498	0.038214	0.000002	0.011853	0.003559	0.006516	0.005770	0.142150	0.000039	0.000309	0.010168	0.000000	0.716407	0.018132	0.000117	1

Table S6C – Pearson correlation coefficients (*R*) for the pooled **Thoracic** segments (ATA + DTA)

	PP	MAP	CD45	CD3	CD68	MMP2	MMP12	MMP13	Thick	AxStch	Disten	Energy	CircStiff	AxStiff	CircStr	AxStr
PP	1															
MAP	0.9792	1														
CD45	0.8529	0.7604	1													
CD3	0.8236	0.7520	0.8727	1												
CD68	0.5857	0.4973	0.8762	0.8243	1											
MMP2	0.6871	0.5970	0.7912	0.6655	0.7349	1										
MMP12	0.6621	0.5924	0.7910	0.4109	0.5470	0.6321	1									
MMP13	0.6971	0.6503	0.6488	0.5631	0.5454	0.9244	0.5593	1								
Thick	0.9067	0.8387	0.9738	0.8313	0.8105	0.8263	0.7975	0.7070	1							
AxStch	-0.7327	-0.6717	-0.7508	-0.7697	-0.5959	-0.5661	-0.5554	-0.5885	-0.6662	1						
Disten	-0.9526	-0.9734	-0.7899	-0.6882	-0.5377	-0.6521	-0.7007	-0.6659	-0.8810	0.6203	1					
Energy	-0.7952	-0.6976	-0.9126	-0.7934	-0.7231	-0.7225	-0.7738	-0.6266	-0.8532	0.9134	0.7130	1				
CircStiff	0.3266	0.4012	0.1849	-0.1693	-0.1096	0.0429	0.6035	0.0569	0.3125	0.0365	-0.5378	-0.1538	1			
AxStiff	-0.3479	-0.2458	-0.5708	-0.1926	-0.4188	-0.5789	-0.7372	-0.3400	-0.6246	0.0507	0.4049	0.4460	-0.5105	1		
CircStr	-0.5611	-0.4166	-0.8504	-0.7898	-0.8194	-0.6612	-0.5976	-0.4789	-0.7252	0.8145	0.4209	0.9072	0.1777	0.3990	1	
AxStr	-0.8099	-0.7177	-0.9159	-0.7902	-0.7237	-0.7436	-0.7846	-0.6536	-0.8660	0.9091	0.7383	0.9987	-0.1795	0.4572	0.8920	1

Legend

PP	Pulse Pressure	**Thick**	Unloaded Thickness
MAP	Mean Arterial Pressure	**AxStch**	Axial Stretch
CD45	CD45+ Cell Density	**Disten**	Distensibility
CD3	CD3+ Cell Density	**Energy**	Stored Energy
CD68	CD68+ Cell Density	**CircStiff**	Circumferential Stiffness
MMP2	MMP2+ Area	**AxStiff**	Axial Stiffness
MMP12	MMP12+ Area	**CircStr**	Circumferential Stress
MMP13	MMP13+ Area	**AxStr**	Axial Stress

Table S6D – Correlation *p*-values for the pooled **Thoracic** segments (ATA + DTA)

	PP	MAP	CD45	CD3	CD68	MMP2	MMP12	MMP13	Thick	AxStch	Disten	Energy	CircStiff	AxStiff	CircStr	AxStr
PP	1															
MAP	0.000022	1														
CD45	0.007108	0.028489	1													
CD3	0.011974	0.031392	0.004681	1												
CD68	0.127139	0.209901	0.004317	0.011841	1											
MMP2	0.059713	0.118158	0.019352	0.071662	0.037801	1										
MMP12	0.073686	0.121744	0.019407	0.311862	0.160588	0.092643	1									
MMP13	0.054654	0.080812	0.081785	0.146117	0.162095	0.001021	0.149501	1								
Thick	0.001890	0.009261	0.000044	0.010544	0.014682	0.011460	0.017726	0.049889	1							
AxStch	0.038696	0.068106	0.031833	0.025518	0.118985	0.143540	0.152919	0.124846	0.071247	1						
Disten	0.000257	0.000046	0.019684	0.059179	0.169241	0.079707	0.052899	0.071452	0.003843	0.100820	1					
Energy	0.018311	0.054389	0.001562	0.018775	0.042648	0.042931	0.024254	0.096460	0.007059	0.001518	0.047124	1				
CircStiff	0.429755	0.324523	0.661051	0.688553	0.796213	0.919704	0.113136	0.893491	0.451167	0.931534	0.169184	0.716073	1			
AxStiff	0.398452	0.557270	0.139464	0.647742	0.301700	0.132673	0.036907	0.409921	0.097788	0.905103	0.319680	0.268073	0.196106	1		
CircStr	0.147913	0.304521	0.007456	0.019719	0.012806	0.074198	0.117705	0.229938	0.041773	0.013823	0.299126	0.001860	0.673776	0.327543	1	
AxStr	0.014812	0.044995	0.001396	0.019606	0.042389	0.034454	0.021132	0.078761	0.005425	0.001754	0.036484	0.000000	0.670516	0.254687	0.002897	1

Table S6E – Pearson correlation coefficients (*R*) for the pooled A**bdominal** segments (SAA + IAA)

	PP	MAP	CD45	CD3	CD68	MMP2	MMP12	MMP13	Thick	AxStch	Disten	Energy	CircStiff	AxStiff	CircStr	AxStr
PP	1															
MAP	0.9792	1														
CD45	0.7441	0.6409	1													
CD3	0.7777	0.7508	0.4004	1												
CD68	0.7101	0.6766	0.6956	0.5389	1											
MMP2	0.5819	0.6284	0.3976	0.7061	0.6593	1										
MMP12	0.1625	0.2211	0.0950	0.2382	0.5386	0.6362	1									
MMP13	-0.1104	-0.0099	-0.3736	0.0775	-0.4015	0.2507	-0.1412	1								
Thick	0.7189	0.6359	0.9838	0.3176	0.6815	0.3747	0.0811	-0.3996	1							
AxStch	-0.5543	-0.4991	-0.6533	-0.2217	-0.2664	-0.0183	0.4705	0.3164	-0.7240	1						
Disten	-0.8953	-0.9120	-0.7150	-0.5896	-0.6910	-0.6704	-0.3543	-0.0968	-0.6943	0.3244	1					
Energy	-0.3937	-0.2782	-0.7975	-0.2637	-0.6340	-0.4413	-0.4721	0.4042	-0.7380	0.1407	0.4816	1				
CircStiff	0.3887	0.5055	-0.1268	0.1482	-0.0807	-0.0333	-0.3256	0.3636	-0.0651	-0.3041	-0.3458	0.6277	1			
AxStiff	0.0660	0.2112	-0.5958	0.2582	-0.2402	0.1319	0.0927	0.5792	-0.6051	0.3970	-0.0899	0.6843	0.6768	1		
CircStr	-0.0376	0.0852	-0.5360	-0.0617	-0.4233	-0.2856	-0.4787	0.3956	-0.4662	-0.1165	0.1447	0.9250	0.8694	0.7276	1	
AxStr	-0.3997	-0.2665	-0.8879	-0.1651	-0.5736	-0.2850	-0.2138	0.4953	-0.8605	0.4185	0.4213	0.9432	0.5519	0.8376	0.8371	1

Legend

PP	Pulse Pressure	**Thick**	Unloaded Thickness
MAP	Mean Arterial Pressure	**AxStch**	Axial Stretch
CD45	CD45+ Cell Density	**Disten**	Distensibility
CD3	CD3+ Cell Density	**Energy**	Stored Energy
CD68	CD68+ Cell Density	**CircStiff**	Circumferential Stiffness
MMP2	MMP2+ Area	**AxStiff**	Axial Stiffness
MMP12	MMP12+ Area	**CircStr**	Circumferential Stress
MMP13	MMP13+ Area	**AxStr**	Axial Stress

Table S6F – Correlation *p*-values for the pooled **Abdominal** segments (SAA + IAA)

	PP	MAP	CD45	CD3	CD68	MMP2	MMP12	MMP13	Thick	AxStch	Disten	Energy	CircStiff	AxStiff	CircStr	AxStr
PP	1															
MAP	0.000022	1														
CD45	0.034251	0.086851	1													
CD3	0.023102	0.031803	0.325676	1												
CD68	0.048424	0.065351	0.055412	0.168178	1											
MMP2	0.130188	0.095208	0.329344	0.050280	0.075299	1										
MMP12	0.700642	0.598757	0.822961	0.570050	0.168426	0.089936	1									
MMP13	0.794667	0.981420	0.361928	0.855315	0.324235	0.549269	0.738712	1								
Thick	0.044485	0.090147	0.000011	0.443272	0.062732	0.360487	0.848680	0.326671	1							
AxStch	0.153974	0.207956	0.078994	0.597765	0.523585	0.965631	0.239400	0.445174	0.042267	1						
Disten	0.002648	0.001595	0.046223	0.123949	0.057705	0.068840	0.389146	0.819710	0.056071	0.433042	1					
Energy	0.334509	0.504699	0.017747	0.528041	0.091405	0.273716	0.237491	0.320584	0.036584	0.739566	0.226950	1				
CircStiff	0.341219	0.201262	0.764810	0.726140	0.849322	0.937597	0.431256	0.375992	0.878315	0.463980	0.401417	0.095694	1			
AxStiff	0.876615	0.615689	0.119128	0.536964	0.566605	0.755482	0.827245	0.132456	0.111992	0.330126	0.832337	0.061203	0.065286	1		
CircStr	0.929554	0.841066	0.170863	0.884698	0.296079	0.492946	0.230078	0.332051	0.244320	0.783533	0.732466	0.000996	0.005035	0.040768	1	
AxStr	0.326534	0.523545	0.003231	0.696102	0.137103	0.493848	0.611215	0.212043	0.006095	0.302182	0.298619	0.000440	0.156105	0.009441	0.009533	1

Table S6G – Pearson correlation coefficients (*R*) for the **ATA**

	PP	MAP	CD45	CD3	CD68	MMP2	MMP12	MMP13	Thick	AxStch	Disten	Energy	CircStiff	AxStiff	CircStr	AxStr
PP	1															
MAP	0.9792	1														
CD45	0.9163	0.8567	1													
CD3	0.9790	0.9197	0.9591	1												
CD68	0.7522	0.7312	0.9231	0.7864	1											
MMP2	0.8592	0.8218	0.6321	0.8254	0.3179	1										
MMP12	0.8661	0.8057	0.9930	0.9191	0.9559	0.5363	1									
MMP13	0.8298	0.7891	0.5939	0.7973	0.2677	0.9984	0.4951	1								
Thick	0.9874	0.9613	0.9643	0.9825	0.8461	0.7726	0.9317	0.7373	1							
AxStch	-0.9456	-0.8858	-0.9956	-0.9814	-0.8863	-0.7020	-0.9776	-0.6668	-0.9794	1						
Disten	-0.9472	-0.9910	-0.8294	-0.8718	-0.7498	-0.7488	-0.7864	-0.7119	-0.9375	0.8516	1					
Energy	-0.9342	-0.8760	-0.9987	-0.9719	-0.9060	-0.6698	-0.9858	-0.6329	-0.9746	0.9990	0.8458	1				
CircStiff	0.6822	0.7721	0.7033	0.6047	0.8424	0.2750	0.7199	0.2225	0.7408	-0.6777	-0.8430	-0.6958	1			
AxStiff	-0.9322	-0.8652	-0.9967	-0.9766	-0.8887	-0.6853	-0.9815	-0.6504	-0.9698	0.9991	0.8286	0.9987	-0.6587	1		
CircStr	-0.7527	-0.6367	-0.9393	-0.8616	-0.8653	-0.4760	-0.9526	-0.4445	-0.8244	0.9218	0.5882	0.9286	-0.4858	0.9375	1	
AxStr	-0.9502	-0.8993	-0.9955	-0.9782	-0.8974	-0.6948	-0.9783	-0.6580	-0.9847	0.9989	0.8708	0.9987	-0.7108	0.9965	0.9089	1

Legend

PP	Pulse Pressure	**Thick**	Unloaded Thickness
MAP	Mean Arterial Pressure	**AxStch**	Axial Stretch
CD45	CD45+ Cell Density	**Disten**	Distensibility
CD3	CD3+ Cell Density	**Energy**	Stored Energy
CD68	CD68+ Cell Density	**CircStiff**	Circumferential Stiffness
MMP2	MMP2+ Area	**AxStiff**	Axial Stiffness
MMP12	MMP12+ Area	**CircStr**	Circumferential Stress
MMP13	MMP13+ Area	**AxStr**	Axial Stress

Table S6H – Correlation *p*-values for the **ATA**

	PP	MAP	CD45	CD3	CD68	MMP2	MMP12	MMP13	Thick	AxStch	Disten	Energy	CircStiff	AxStiff	CircStr	AxStr
PP	1															
MAP	0.020776	1														
CD45	0.083722	0.143271	1													
CD3	0.021020	0.080337	0.040903	1												
CD68	0.247834	0.268832	0.076930	0.213646	1											
MMP2	0.140810	0.178214	0.367924	0.174608	0.682053	1										
MMP12	0.133854	0.194256	0.007001	0.080903	0.044086	0.463749	1									
MMP13	0.170204	0.210877	0.406128	0.202670	0.732284	0.001560	0.504943	1								
Thick	0.012624	0.038668	0.035674	0.017495	0.153873	0.227428	0.068259	0.262712	1							
AxStch	0.054354	0.114168	0.004416	0.018567	0.113652	0.298008	0.022434	0.333227	0.020648	1						
Disten	0.052799	0.008998	0.170563	0.128151	0.250168	0.251214	0.213567	0.288062	0.062472	0.148403	1					
Energy	0.065810	0.124040	0.001258	0.028115	0.094032	0.330175	0.014156	0.367060	0.025408	0.001019	0.154184	1				
CircStiff	0.317792	0.227872	0.296710	0.395291	0.157640	0.724976	0.280115	0.777491	0.259168	0.322270	0.157001	0.304212	1			
AxStiff	0.067776	0.134772	0.003325	0.023448	0.111320	0.314733	0.018469	0.349609	0.030184	0.000918	0.171428	0.001277	0.341258	1		
CircStr	0.247339	0.363285	0.060678	0.138443	0.134664	0.523967	0.047393	0.555517	0.175553	0.078198	0.411793	0.071353	0.514216	0.062542	1	
AxStr	0.049824	0.100658	0.004524	0.021814	0.102553	0.305205	0.021748	0.342000	0.015293	0.001102	0.129170	0.001294	0.289192	0.003493	0.091064	1

Table S6I – Pearson correlation coefficients (*R*) for the **DTA**

	PP	MAP	CD45	CD3	CD68	MMP2	MMP12	MMP13	Thick	AxStch	Disten	Energy	CircStiff	AxStiff	CircStr	AxStr
PP	1															
MAP	0.9792	1														
CD45	0.8185	0.6996	1													
CD3	0.9312	0.8385	0.9569	1												
CD68	0.6572	0.5302	0.9594	0.8375	1											
MMP2	0.5327	0.3940	0.9096	0.7499	0.9880	1										
MMP12	0.5221	0.4108	0.8693	0.6976	0.9712	0.9827	1									
MMP13	0.5345	0.4771	0.7784	0.6181	0.8906	0.8889	0.9572	1								
Thick	0.8725	0.7704	0.9944	0.9742	0.9360	0.8722	0.8409	0.7722	1							
AxStch	-0.8577	-0.7427	-0.9948	-0.9806	-0.9258	-0.8640	-0.8148	-0.7198	-0.9951	1						
Disten	-0.9876	-0.9816	-0.8113	-0.9003	-0.6799	-0.5603	-0.5774	-0.6254	-0.8684	0.8389	1					
Energy	-0.6640	-0.5009	-0.9501	-0.8905	-0.9140	-0.8913	-0.8025	-0.6299	-0.9181	0.9467	0.6215	1				
CircStiff	-0.0052	0.1960	-0.5391	-0.3694	-0.6234	-0.7006	-0.5846	-0.3356	-0.4488	0.5038	-0.0474	0.7504	1			
AxStiff	-0.2982	-0.1026	-0.7684	-0.6245	-0.8173	-0.8580	-0.7550	-0.5329	-0.6979	0.7399	0.2553	0.9114	0.9532	1		
CircStr	-0.4714	-0.2867	-0.8707	-0.7594	-0.8847	-0.8980	-0.8011	-0.5986	-0.8161	0.8519	0.4297	0.9721	0.8816	0.9824	1	
AxStr	-0.6712	-0.5107	-0.9586	-0.8940	-0.9282	-0.9056	-0.8229	-0.6580	-0.9276	0.9527	0.6343	0.9993	0.7415	0.9076	0.9701	1

Legend

PP	Pulse Pressure	**Thick**	Unloaded Thickness
MAP	Mean Arterial Pressure	**AxStch**	Axial Stretch
CD45	CD45+ Cell Density	**Disten**	Distensibility
CD3	CD3+ Cell Density	**Energy**	Stored Energy
CD68	CD68+ Cell Density	**CircStiff**	Circumferential Stiffness
MMP2	MMP2+ Area	**AxStiff**	Axial Stiffness
MMP12	MMP12+ Area	**CircStr**	Circumferential Stress
MMP13	MMP13+ Area	**AxStr**	Axial Stress

Table S6J–Correlation *p*-values for the **DTA**

	PP	MAP	CD45	CD3	CD68	MMP2	MMP12	MMP13	Thick	AxStch	Disten	Energy	CircStiff	AxStiff	CircStr	AxStr
PP	1															
MAP	0.020776	1														
CD45	0.181469	0.300441	1													
CD3	0.068818	0.161485	0.043068	1												
CD68	0.342834	0.469768	0.040626	0.162544	1											
MMP2	0.467318	0.605999	0.090353	0.250121	0.012037	1										
MMP12	0.477898	0.589193	0.130707	0.302443	0.028845	0.017276	1									
MMP13	0.465487	0.522907	0.221610	0.381858	0.109386	0.111084	0.042840	1								
Thick	0.127518	0.229582	0.005571	0.025820	0.063992	0.127802	0.159138	0.227796	1							
AxStch	0.142316	0.257282	0.005193	0.019437	0.074244	0.135974	0.185249	0.280195	0.004893	1						
Disten	0.012410	0.018444	0.188691	0.099698	0.320112	0.439730	0.422647	0.374618	0.131589	0.161061	1					
Energy	0.336037	0.499105	0.049873	0.109452	0.085954	0.108710	0.197481	0.370063	0.081878	0.053335	0.378480	1				
CircStiff	0.994832	0.804023	0.460933	0.630641	0.376609	0.299351	0.415430	0.664409	0.551165	0.496199	0.952579	0.249587	1			
AxStiff	0.701845	0.897435	0.231606	0.375502	0.182660	0.141972	0.244961	0.467073	0.302123	0.260060	0.744713	0.088628	0.046758	1		
CircStr	0.528581	0.713278	0.129331	0.240606	0.115299	0.102009	0.198928	0.401364	0.183911	0.148119	0.570313	0.027903	0.118414	0.017648	1	
AxStr	0.328762	0.489256	0.041394	0.105986	0.071769	0.094381	0.177134	0.342044	0.072416	0.047295	0.365660	0.000676	0.258508	0.092434	0.029923	1

Table S6K – Pearson correlation coefficients (*R*) for the **SAA**

	PP	MAP	CD45	CD3	CD68	MMP2	MMP12	MMP13	Thick	AxStch	Disten	Energy	CircStiff	AxStiff	CircStr	AxStr
PP	1															
MAP	0.9792	1														
CD45	0.7604	0.6395	1													
CD3	0.7951	0.9004	0.3260	1												
CD68	0.8544	0.7337	0.9561	0.3836	1											
MMP2	0.4459	0.5163	0.4496	0.6581	0.2699	1										
MMP12	0.1043	-0.0211	0.7023	-0.2160	0.4845	0.4406	1									
MMP13	0.0624	0.2568	-0.3527	0.6505	-0.4084	0.6128	-0.3784	1								
Thick	0.7506	0.6329	0.9992	0.3303	0.9442	0.4807	0.7211	-0.3295	1							
AxStch	-0.8307	-0.7319	-0.9907	-0.4514	-0.9563	-0.5220	-0.6341	0.2374	-0.9907	1						
Disten	-0.9748	-0.9763	-0.7622	-0.8558	-0.8001	-0.6339	-0.1905	-0.2141	-0.7614	0.8421	1					
Energy	-0.4325	-0.2763	-0.9144	0.0474	-0.7972	-0.3371	-0.9072	0.5368	-0.9190	0.8571	0.4484	1				
CircStiff	0.4451	0.5887	-0.2414	0.7662	-0.0558	0.1063	-0.7922	0.6315	-0.2523	0.1195	-0.4201	0.6132	1			
AxStiff	-0.0890	0.0889	-0.7087	0.4097	-0.5707	-0.0910	-0.9213	0.7070	-0.7128	0.6110	0.0893	0.9298	0.8509	1		
CircStr	-0.0977	0.0701	-0.7201	0.3657	-0.5613	-0.1784	-0.9538	0.6375	-0.7278	0.6284	0.1187	0.9392	0.8471	0.9956	1	
AxStr	-0.4321	-0.2736	-0.9139	0.0556	-0.8007	-0.3207	-0.9021	0.5512	-0.9178	0.8554	0.4439	0.9998	0.6145	0.9321	0.9397	1

Legend

PP	Pulse Pressure	**Thick**	Unloaded Thickness
MAP	Mean Arterial Pressure	**AxStch**	Axial Stretch
CD45	CD45+ Cell Density	**Disten**	Distensibility
CD3	CD3+ Cell Density	**Energy**	Stored Energy
CD68	CD68+ Cell Density	**CircStiff**	Circumferential Stiffness
MMP2	MMP2+ Area	**AxStiff**	Axial Stiffness
MMP12	MMP12+ Area	**CircStr**	Circumferential Stress
MMP13	MMP13+ Area	**AxStr**	Axial Stress

Table S6L –Correlation *p*-values for the **SAA**

	PP	MAP	CD45	CD3	CD68	MMP2	MMP12	MMP13	Thick	AxStch	Disten	Energy	CircStiff	AxStiff	CircStr	AxStr
PP	1															
MAP	0.020776	1														
CD45	0.239578	0.360518	1													
CD3	0.204860	0.099589	0.673963	1												
CD68	0.145621	0.266350	0.043901	0.616401	1											
MMP2	0.554123	0.483656	0.550354	0.341875	0.730079	1										
MMP12	0.895727	0.978877	0.297747	0.783967	0.515522	0.559368	1									
MMP13	0.937551	0.743222	0.647322	0.349486	0.591648	0.387158	0.621647	1								
Thick	0.249417	0.367121	0.000837	0.669722	0.055840	0.519267	0.278877	0.670542	1							
AxStch	0.169309	0.268089	0.009270	0.548631	0.043665	0.477982	0.365856	0.762563	0.009275	1						
Disten	0.025155	0.023702	0.237757	0.144175	0.199921	0.366051	0.809486	0.785851	0.238552	0.157944	1					
Energy	0.567488	0.723718	0.085604	0.952634	0.202811	0.662855	0.092836	0.463236	0.081039	0.142947	0.551601	1				
CircStiff	0.554908	0.411280	0.758589	0.233840	0.944162	0.893727	0.207804	0.368536	0.747690	0.880532	0.579883	0.386792	1			
AxStiff	0.911045	0.911065	0.291286	0.590289	0.429313	0.909028	0.078732	0.292960	0.287164	0.389038	0.910749	0.070167	0.149142	1		
CircStr	0.902255	0.929922	0.279856	0.634275	0.438745	0.821588	0.046215	0.362517	0.272152	0.371572	0.881296	0.060761	0.152908	0.004449	1	
AxStr	0.567945	0.726388	0.086072	0.944440	0.199269	0.679307	0.097908	0.448833	0.082213	0.144636	0.556122	0.000170	0.385497	0.067937	0.060264	1

Table S6M – Pearson correlation coefficients (*R*) for the **IAA**

	PP	MAP	CD45	CD3	CD68	MMP2	MMP12	MMP13	Thick	AxStch	Disten	Energy	CircStiff	AxStiff	CircStr	AxStr
PP	1															
MAP	0.9792	1														
CD45	0.9291	0.8372	1													
CD3	0.9569	0.8836	0.9948	1												
CD68	0.6137	0.6532	0.5474	0.6102	1											
MMP2	0.8127	0.8449	0.7177	0.7783	0.9567	1										
MMP12	0.3026	0.4777	-0.0086	0.0936	0.6612	0.6365	1									
MMP13	-0.6754	-0.7946	-0.4234	-0.5137	-0.8334	-0.8853	-0.9023	1								
Thick	0.9895	0.9594	0.9488	0.9758	0.6975	0.8654	0.3025	-0.6833	1							
AxStch	-0.9496	-0.8716	-0.9736	-0.9693	-0.4157	-0.6360	0.0108	0.4107	-0.9360	1						
Disten	-0.9374	-0.9880	-0.7434	-0.8008	-0.6329	-0.8232	-0.5791	0.8462	-0.9056	0.7962	1					
Energy	-0.7964	-0.6931	-0.9327	-0.9268	-0.6979	-0.7705	0.0011	0.4000	-0.8667	0.8258	0.5808	1				
CircStiff	0.5051	0.6306	0.1788	0.2404	0.0770	0.2847	0.5744	-0.6000	0.3938	-0.3548	-0.7281	0.1169	1			
AxStiff	0.5410	0.6749	0.2055	0.2753	0.1864	0.3786	0.6588	-0.6878	0.4412	-0.3633	-0.7731	0.0641	0.9932	1		
CircStr	0.1633	0.3072	-0.1702	-0.1164	-0.2114	-0.0456	0.4798	-0.3640	0.0360	-0.0298	-0.4321	0.4661	0.9323	0.9031	1	
AxStr	-0.6607	-0.5049	-0.8896	-0.8497	-0.4265	-0.5104	0.3383	0.0761	-0.7235	0.7950	0.3659	0.9411	0.2827	0.2630	0.5810	1

Legend

PP	Pulse Pressure	**Thick**	Unloaded Thickness
MAP	Mean Arterial Pressure	**AxStch**	Axial Stretch
CD45	CD45+ Cell Density	**Disten**	Distensibility
CD3	CD3+ Cell Density	**Energy**	Stored Energy
CD68	CD68+ Cell Density	**CircStiff**	Circumferential Stiffness
MMP2	MMP2+ Area	**AxStiff**	Axial Stiffness
MMP12	MMP12+ Area	**CircStr**	Circumferential Stress
MMP13	MMP13+ Area	**AxStr**	Axial Stress

Table S6N –Correlation *p*-values for the **IAA**

	PP	MAP	CD45	CD3	CD68	MMP2	MMP12	MMP13	Thick	AxStch	Disten	Energy	CircStiff	AxStiff	CircStr	AxStr
PP	1															
MAP	0.020776	1														
CD45	0.070882	0.162771	1													
CD3	0.043085	0.116441	0.005241	1												
CD68	0.386252	0.346834	0.452586	0.389814	1											
MMP2	0.187305	0.155141	0.282301	0.221669	0.043300	1										
MMP12	0.697395	0.522257	0.991394	0.906424	0.338837	0.363478	1									
MMP13	0.324608	0.205392	0.576629	0.486299	0.166561	0.114714	0.097726	1								
Thick	0.010547	0.040613	0.051180	0.024154	0.302487	0.134561	0.697501	0.316661	1							
AxStch	0.050358	0.128357	0.026408	0.030687	0.584349	0.363971	0.989224	0.589264	0.064027	1						
Disten	0.062558	0.011954	0.256611	0.199191	0.367102	0.176831	0.420936	0.153835	0.094410	0.203821	1					
Energy	0.203592	0.306865	0.067279	0.073152	0.302089	0.229545	0.998857	0.600009	0.133335	0.174230	0.419187	1				
CircStiff	0.494942	0.369434	0.821217	0.759592	0.922959	0.715302	0.425634	0.400042	0.606172	0.645213	0.271927	0.883119	1			
AxStiff	0.458975	0.325097	0.794479	0.724698	0.813567	0.621398	0.341172	0.312230	0.558785	0.636660	0.226934	0.935923	0.006807	1		
CircStr	0.836724	0.692845	0.829778	0.883560	0.788637	0.954372	0.520244	0.636036	0.964021	0.970198	0.567887	0.533912	0.067704	0.096940	1	
AxStr	0.339340	0.495136	0.110371	0.150283	0.573537	0.489628	0.661688	0.923915	0.276507	0.204979	0.634124	0.058936	0.717339	0.736956	0.419029	1